Mercurophilic interactions in heterometallic Ru-Hg carbonyl clusters

Mercurophilic Interactions in Heterometallic Ru-Hg carbonyl clusters†

Cristiana Cesari,[a]* Marco Bortoluzzi,[b] Cristina Femoni,[a] Maria Carmela Iapalucci,[a] and Stefano Zacchini[a]*

[a] Dipartimento di Chimica Industriale "Toso Montanari", Università di Bologna, Viale Risorgimento 4 - 40136 Bologna. Italy. E-mail: stefano.zacchini@unibo.it

[b] Dipartimento di Scienze Molecolari e Nanosistemi, Ca' Foscari University of Venice, Via Torino 155 – 30175 Mestre (Ve), Italy.

† Dedicated to Professor R. Bruce King in recognition of his contributions to inorganic, organometallic and cluster chemistry

Abstract: The reaction of $[HRu_3(CO)_{11}]^-$ (**1**) with 0.35 mole equivalents of $Hg(CH_3CO_2)_2$ afforded $[HgRu_6(CO)_{22}]^{2-}$ (**3**), whereas a mixture of **3** and $[Hg_2Ru_7(CO)_{26}]^{2-}$ (**4**) was obtained using 0.5 mole equivalents of $Hg(CH_3CO_2)_2$ per mole of **1**. A few crystals of $[Ru_3(CO)_{10}(CH_3COO)]^-$ (**7**) were obtained as side products of the latter reaction. The reaction of **1** with one mole equivalent of $Hg(CH_3CO_2)_2$ or $HgCl_2$ afforded $[Hg_3Ru_8(CO)_{30}]^{2-}$ (**5**) as the major product. By employing $HgCl_2$, formation of **5** was accompanied by traces of the new homometallic cluster $[Ru_2Cl_4(CO)_5]^{2-}$ (**8**). $[HRu_4(CO)_{12}]^{3-}$ (**2**) reacted with one mole equivalent of $HgCl_2$ resulting in $[Hg_4Ru_{10}(CO)_{32}]^{4-}$ (**6**). The molecular structures of the new clusters **3-8** were determined by single crystal X-ray diffraction (SC-XRD) as their $[NEt_4]_2$[**3**], $[NEt_4]_2$[**4**]·$0.5CH_2Cl_2$, $[NEt_4]_2$[**5**], $[NEt_4]_4$[**6**], $[NEt_4]$[**7**], $[NEt_4]_2$[**8**]·$0.5CH_3CN$ salts. Heterometallic Ru-Hg clusters **3-6** contain $[Hg]^{2+}$, $[Hg_2]^{4+}$, $[Hg_3]^{6+}$, and $[Hg_4]^{8+}$ cores stabilized by $[Ru(CO)_4]^{2-}$, $[Ru_3CO)_{11}]^{2-}$ and $[Ru_4(CO)_{12}]^{4-}$ fragments. Metal-metal bonds were investigated by DFT calculations and atoms-in-molecules (AIM) analyses.

Keywords: Cluster Compounds; Carbonyl Ligands; Mercurophilic Interactions; Computational Investigations; Heterometallic Bonds

1. Introduction

Attractive interactions between d^{10} closed-electron-shell metal ions are usually referred as metallophilic interactions.[1-6] Metallophilicity has been widely experimentally and theoretically explored, with particular regard to M(I) (M = Cu, Ag, Au) coinage metal ions. Indeed, this phenomenon was first discovered for Au(I) ions, and thus referred as aurophilicity [7-13]. Then, it was extended to Ag(I) (argentophilicity) [14] and Cu(I) (cuprophilicity) [15] and, eventually, also to Hg(II) (mercurophilicity) [16-19]. Their nature is still debated, but there are nowadays numerous examples of compounds containing both inter-molecular and intra-molecular metallophilic interactions.

Among the different classes of inorganic and organometallic compounds displaying metallophilicity, some interesting examples have been also reported for heterometallic carbonyl clusters [20-28]. In addition, heterometallic clusters can be employed for the activation of small organic molecules [29-38], for applications in homeogeneous catalysis and as precursors of metal nanoparticles and heterogeneous nanostructured catalysts [39-52].

The first example of a metal carbonyl compound displaying a weak Hg(II)···Hg(II) mercurophilic interaction was probably $Fe(CO)_4(HgCl)_2$, which was discovered in 1928 [53]. The structure of the related $Fe(CO)_4(HgBr)_2$ was determined by single crystal X-ray diffraction (SC-XRD) 40 years later, revealing the presence in the unit cell of two independent molecules with Hg(II)···Hg(II) contacts of 2.97 and 3.12 Å, well below that proposed for van der Waals contacts (*ca*. 3.5 Å) [54]. Dimeric $[Hg_2]^{4+}$ units not supported by ancillary ligands and showing sub van der Waals Hg(II)···Hg(II) contacts have been, then, found in *cis*-$[Os(CO)_4\{(\mu\text{-}Hg)Os_3(CO)_{10}(\mu\text{-}Cl)\}_2]$ (3.54-3.59 Å) [55], $[Hg_2Os_{18}(C)_2(CO)_{42}]^{4-}$ (2.82 Å) [56] and $[Hg_2Os_{18}(C)_2(CO)_{42}]^{2-}$ (2.74 Å), even though the rather short contact found in the latter compound is likely to be due to unresolved disorder [57]. An even shorter contact is present in $[Hg_2Re_{14}(C)_2(CO)_{42}]^{4-}$ (2.61 Å), but this contains Hg(I) instead of Hg(II), and the cluster may be partitioned into two $[Re_7C(CO)_{21}]^{3-}$ units and one covalently bonded $[Hg_2]^{2+}$ dimer [58]. It is noteworthy that $Hg_2Pt_6(CO)_6(PPh^iPr_2)_6$ is composed of two $Pt_3(\mu\text{-}CO)_3(PPh^iPr_2)_3$ triangular units joined by a Hg_2 dimer [59]. No formal oxidation state has been assigned to Hg in the original paper, even though the Hg···Hg contact (3.22 Å) is in keeping with a mercurophilic Hg(II)···Hg(II) interaction. This would correspond to the assignment of a dianionic charge to each Pt_3 unit, as found in Chini clusters [60].

Triangular $[Hg_3]^{6+}$ trimers are present in $Hg_3Os_9(CO)_{33}$ [61] and $[Hg_3Os_{18}(C)_2(CO)_{42}]^{2-}$ [62], showing Hg(II)···Hg(II) mercurophilic contacts of 3.08-3.12 and 2.92-2.93 Å, respectively. Square $[Hg_4]^{4+}$ tetramers are present in the structures of $Hg_4Ru_4(CO)_{16}$ [63] and $Hg_4Mn_4(MeCp)_4(CO)_8$ [64], the former displaying very long Hg(II)···Hg(II) contacts of 3.52 Å, whereas the latter

heteroleptic compound shows rather short mercurophilic interactions of 2.89 Å. Even if its synthesis was reported long time ago, the structure of $Hg_4Fe_4(CO)_{16}$ [65] is not yet known. This compound is probably isostructural to $Cd_4Fe_4(CO)_{16}$ [66], showing a square $[Hg_4]^{4+}$ core.

The ability of Hg(II) in these clusters to serve as acceptor site is further supported by the heteroleptic $Hg_4Fe_4(L)_2(CO)_{12}$ (L = 2,6-bis(disphenylphosphino)pyridine) complex [67]. The interaction of the pyridine ligands with two Hg(II) sites elongates the $[Hg_4]^{4+}$ core, which shows two shorter (3.41 Å) and two longer (3.52 Å) Hg(II)···Hg(II) contacts.

The largest mercury unit found within a carbonyl cluster is the Hg_8 octa-nuclear framework present in $[Hg_8Ir_6(Cp^*)_6(CO)_6]^{6+}$ [68]. The Hg···Hg contacts are in the range 2.96-3.08 Å in keeping with mercurophilic interactions, but in this case it is not possible to easily assign a formal oxidation state to Hg. Indeed, the assignment of formal oxidation states to atoms within metal clusters is not a trivial task, and often it can be rationalized in multiple ways. Even when a tentative assignment is possible, it must be considered as a formal and simplistic bonding model, and there are often more than one interpretation available.

Within this framework, this paper reports the synthesis of four new Ru-Hg carbonyl clusters containing from one to four Hg(II) ions, that is $[HgRu_6(CO)_{22}]^{2-}$, $[Hg_2Ru_7(CO)_{26}]^{2-}$, $[Hg_3Ru_8(CO)_{30}]^{2-}$ and $[Hg_4Ru_{10}(CO)_{32}]^{4-}$. Their structure have been determined by SC-XRD and the bonding analyzed by computational methods. Mercurophilic interactions are present within the $[Hg_2]^{4+}$, $[Hg_3]^{6+}$ and $[Hg_4]^{8+}$ units composing the cores of such clusters.

2. Results and Discussion

2.1 Synthesis

The reactions of $[HRu_3(CO)_{11}]^-$ (**1**) and $[HRu_4(CO)_{12}]^{3-}$ (**2**) with Hg(II) salts such as $Hg(CH_3CO_2)_2$ and $HgCl_2$ under different experimental conditions (Scheme 1) afforded the new heterometallic Ru-Hg clusters $[HgRu_6(CO)_{22}]^{2-}$ (**3**), $[Hg_2Ru_7(CO)_{26}]^{2-}$ (**4**), $[Hg_3Ru_8(CO)_{30}]^{2-}$ (**5**) and $[Hg_4Ru_{10}(CO)_{32}]^{4-}$ (**6**). Details are reported below, whereas their molecular structures determined by SC-XRD are described in Section 2.2.

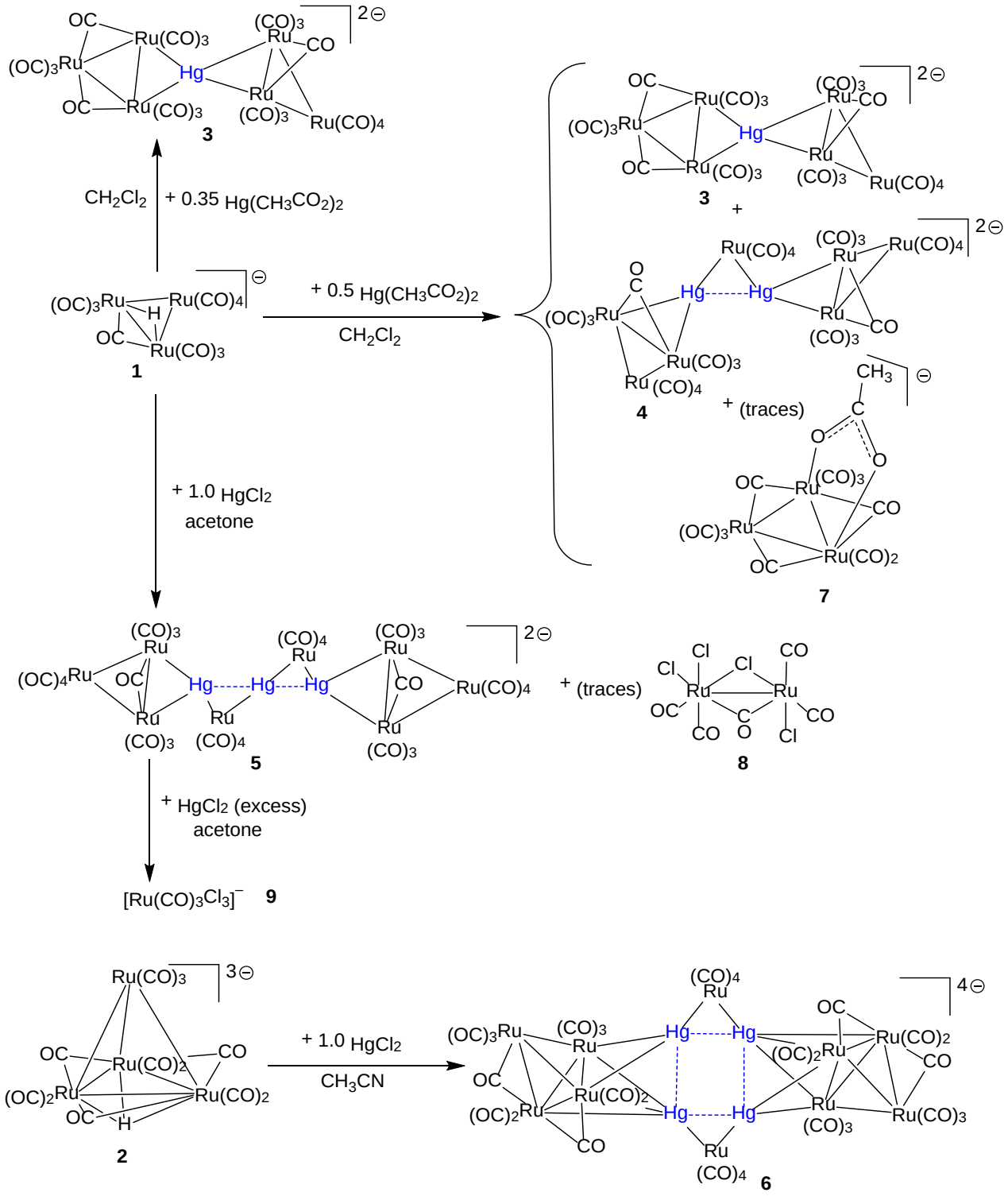

Scheme 1. Synthesis of **3-6**.

The reaction of **1** with a sub-stoichiometric amount of $Hg(CH_3CO_2)_2$ (0.35 mole equivalents) resulted in **3** (Scheme 1). The reaction formally consists in the addition of one mole of the soft Lewis acid Hg^{2+} to two moles of **1** with concomitant substitution of the hard acid H^+ (equation 1). The latter is trapped by the acetate base.

$$2[HRu_3(CO)_{11}]^- + Hg(CH_3CO_2)_2 \rightarrow [HgRu_6(CO)_{22}]^{2-} + 2CH_3COOH \quad (1)$$

Despite the fact that equation 1 requires 0.5 moles of $Hg(CH_3CO_2)_2$ per mole of **1**, the optimized synthesis of **3** employs 0.35 moles of $Hg(CH_3CO_2)_2$ per mole of **1**. Indeed, by increasing the amount of $Hg(CH_3CO_2)_2$ to 0.5 moles, a 1:1 mixture of **3** and **4** was obtained. Formation of such mixtures was accompanied by traces (a few crystals) of the homometallic cluster $[Ru_3(CO)_{10}(CH_3COO)]^-$ (**7**). This indicates that some decomposition, likely due to redox processes, occurred during the reaction, which also justifies the presence of $Ru(CO)_4$ units within the molecular structure of **4**. By monitoring the reaction by IR, after the first addition of $Hg(CH_3CO_2)_2$ to **1**, compound **3** starts to form, but at some point conversion of **3** into **4** begins to be a competitive reaction.

At the same time, formation of **3** was disfavored by further increasing the amount of $Hg(CH_3CO_2)_2$, due to the formation of **5**. Thus, **4** was always obtained in mixture with **3** or **5**, depending on the amount of $Hg(CH_3CO_2)_2$ employed. The optimized synthesis of **5** required one mole of $Hg(CH_3CO_2)_2$ or $HgCl_2$ per mole of **1**. By employing $HgCl_2$, formation of **5** was accompanied by traces of the new homometallic cluster $[Ru_2Cl_4(CO)_5]^{2-}$ (**8**). Further increasing the amount of $HgCl_2$ resulted in the formation of the previously reported complex $[Ru(CO)_3Cl_3]^-$ (**9**) [69].

The reaction of the tetrahedral homometallic cluster **2** with $HgCl_2$ in a 1:1 ratio resulted in the higher nuclearity heterometallic cluster **6**. Also in this case, increasing the amount of $HgCl_2$ favored the formation of **9**, which contain a Ru(II) centre. Formation of **9** from low valent Ru clusters such as **2** and **3** is likely to be due to the synergic effect of the oxidizing Hg(II) ions and the coordinating chloride ions.

All the new clusters **3-8** have been characterized by IR spectroscopy (see Experimental Section and Figures S1-S4 in the Supporting Information) and their molecular structures determined by SC-XRD as their $[NEt_4]_2$[**3**], $[NEt_4]_2$[**4**]·$0.5CH_2Cl_2$, $[NEt_4]_2$[**5**], $[NEt_4]_4$[**6**], $[NEt_4]$[**7**], $[NEt_4]_2$[**8**]·$0.5CH_3CN$ salts (see Section 2.2).

2.2 Molecular structures and computational investigations

2.2.1 $[HgRu_6(CO)_{22}]^{2-}$ (3)

The cluster anion **3** is composed of two $[Ru_3(CO)_{11}]^{2-}$ units joined by a Hg(II) ion, which adopts a distorted tetrahedral coordination being bonded to four Ru atoms (Figure 1 and Table 1). Similar structures displaying Hg(II) coordinated to two Ru_3 triangular units were previously found in $Hg[Ru_3(CO)_9(\mu_3\text{-}\sigma^1,\eta^2,\eta^2\text{-}C{\equiv}C^tBu)]_2$ [70], $Hg[Ru_3(CO)_9(\mu_3\text{-}2\text{-amino-6-methylpyridine})]_2$ [71],

$Hg[Ru_3(CO)_{10}(\mu\text{-}C{=}OMe)]_2$ [72]. One $[Ru_3(CO)_{11}]^{2-}$ unit displays ten terminal and one μ-CO ligands, whereas the other $[Ru_3(CO)_{11}]^{2-}$ unit possesses nine terminal and two edge bridging carbonyls. Thus, **3** may be also written as $[Hg\{Ru_3(CO)_{10}(\mu\text{-}CO)\}\{Ru_3(CO)_9(\mu\text{-}CO)_2\}]^{2-}$. It must be remarked that the free $[Ru_3(CO)_{11}]^{2-}$ anion displays a $[Ru_3(CO)_{10}(\mu\text{-}CO)]^{2-}$ structure, with a single μ-CO [73].

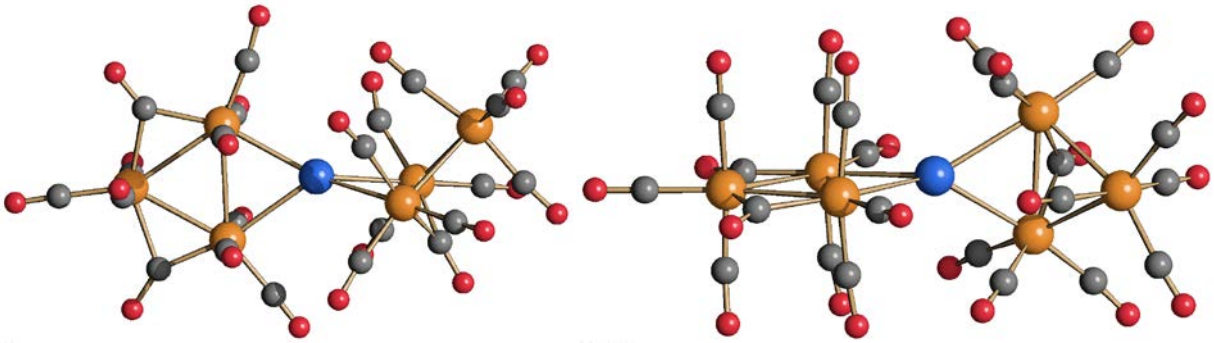

Fig. 1. Two views of the molecular structure of **3** (orange Ru; blue Hg; red O; grey C).

Table 1. Main bond distances (Å) and angles (°) of **3**. Cotton's formal shortness ratios (FSR) are reported in parentheses [74]. Pauling's atomic radii employed [75]: Ru 1.241 Å, Hg 1.440 Å. See Scheme 2 for labeling.

Hg(1)-Ru(1)	2.837(4) *(1.06)*	Hg(1)-Ru(2)	2.791(4) *(1.04)*
Hg(1)-Ru(4)	2.844(4) *(1.06)*	Hg(1)-Ru(5)	2.8425(4) *(1.06)*
Ru(1)-Ru(2)	3.016(5) *(1.22)*	Ru(4)-Ru(5)	2.870(5) *(1.16)*
Ru(1)-Ru(3)	2.863(6) *(1.15)*	Ru(4)-Ru(6)	2.856(5) *(1.15)*
Ru(2)-Ru(3)	2.894(6) *(1.17)*	Ru(5)-Ru(6)	2.841(5) *(1.14)*
$Ru\text{-}CO_{terminal}^{range}$	1.81(6)-2.03(4)	$Ru\text{-}CO_{terminal}^{average}$	1.93(17)
Ru(1)-C(1)	1.94(5)	Ru(3)-C(1)	2.25(6)
Ru(2)-C(2)	2.05(6)	Ru(3)-C(2)	2.11(6)
Ru(4)-C(5)	2.09(4)	Ru(5)-C(3)	2.06(4)
Ru(1)-Hg(1)-Ru(2)	64.82(11)	Ru(4)-Hg(1)-Ru(5)	60.63(10)
Ru(1)-C(1)-O(1)	146(4)	Ru(3)-C(1)-O(1)	128(4)
Ru(2)-C(2)-O(2)	140(4)	Ru(3)-C(2)-O(2)	132(4)
Ru(4)-C(3)-O(3)	137(3)	Ru(5)-C(3)-O(3)	136(3)

$\alpha_{CO(1)}$	0.16(8)	$\alpha_{CO(2)}$	0.03(6)
$\alpha_{CO(3)}$	0.01(6)		

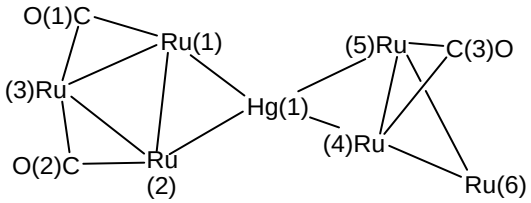

Scheme 2. Labeling of **3**.

The Ru(1)-Ru(2) edge [3.016(5) Å] bridged by Hg(1) and possessing only terminal carbonyls is considerably elongated compared to Ru(4)-Ru(5) [2.870(5) Å] which is bridged both by Hg(1) and a μ-CO ligand. The four Hg-Ru distances [2.791(4)-2.844(4) Å] display a formal shortness ratio (FSR) very close to 1 suggesting the presence of single bonds [74].

The asymmetry parameter (α) of the unique μ-CO of the $[Ru_3(CO)_{10}(\mu\text{-}CO)]^{2-}$ unit of $[HgRu_6(CO)_{22}]^{2-}$ is zero within experimental precision [α = 0.01(6)] as expected for a genuine edge bridging carbonyl [76]. Conversely, within the $[Ru_3(CO)_9(\mu\text{-}CO)_2]^{2-}$ unit, one CO ligand is symmetrically edge bridging [α = 0.03(6)], whereas the second one [α = 0.16(8)] falls in the typical range for semi-bridging carbonyls [α = 0.1-0.6].

The cluster **3** possesses 106 cluster valence electrons (CVE) [6×8 (6Ru) + 1×12 (1Hg) + 22×2 (22CO) + 2 (charge)] as expected on the basis of the effective atomic number (EAN) rule, considering 7 metal atoms and 10 M-M bonds [77].

The DFT-optimized structure of **3** is in good agreement with the X-ray data, the RMSD being 0.283 Å. The computed structure with selected (3,-1) bond critical points (b.c.p.) is shown in Figure 2. The AIM analysis localized four (3,-1) b.c.p.'s related to the Hg-Ru bonds. Data computed at b.c.p. (Table S1 in the Supporting Information) are in line with Bianchi's definition of M-M bonds [78,79]. The electron density values (ρ) at Hg-Ru b.c.p are in the 0.041 - 0.044 a.u. range, with potential energy density (V) values comprised between -0.032 and -0.037 a.u. The interaction of the Hg centre with the $\{Ru_3(CO)_9(\mu\text{-}CO)_2\}$ fragment appears a bit stronger than that with $\{Ru_3(CO)_{10}(\mu\text{-}CO)\}$ on the basis of the slightly more negative V values related to the Hg-Ru interactions. The AIM analysis was unable to localize Ru-Ru b.c.p. between metal centers connected by bridging carbonyl ligands. Three Ru-Ru (3,-1) b.c.p.'s were thus found for compound **3**, the weakest one between Ru(1) and Ru(2) in the $\{Ru_3(CO)_9(\mu\text{-}CO)_2\}$ fragment (Table S1 in the Supporting Information).

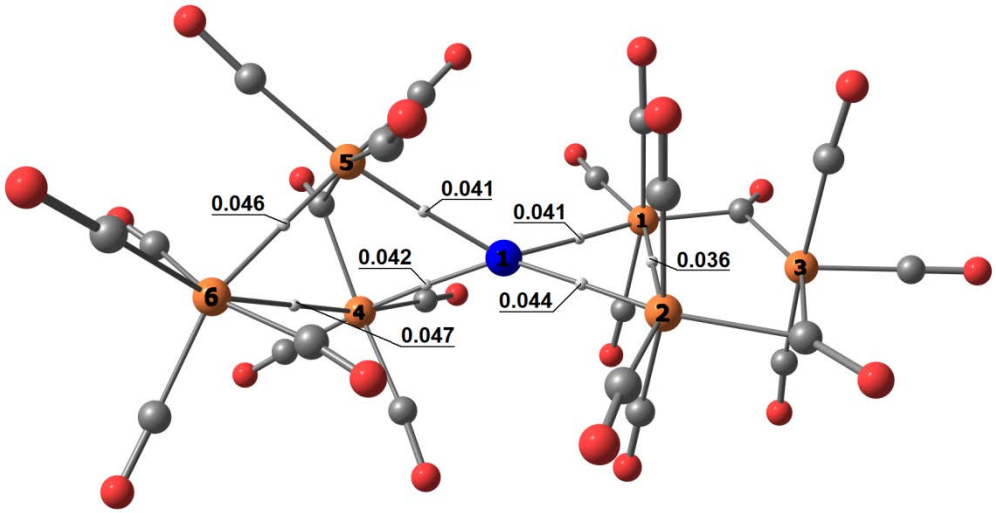

Fig. 2. DFT-optimized structure of **3** (orange Ru; blue Hg; red O; grey C) with localized M-M (3,-1) b.c.p.'s (white) and corresponding electron density values in a.u.

2.2.2 $[Hg_2Ru_7(CO)_{26}]^{2-}$ (4)

The molecular structure of **4** consists of a central $Ru(CO)_4$ fragment bound to two $HgRu_3(CO)_{11}$ butterfly units in a *cis* configuration (Figure 3 and Table 2). It may be partitioned into two Hg(II) cations, two $[Ru_3(CO)_{10}(\mu\text{-}CO)]^{2-}$ cluster anions and one $[Ru(CO)_4]^{2-}$ anion. Each Hg(II) centre is tri-coordinated being bonded to $[Ru(CO)_4]^{2-}$ and to one edge of a $[Ru_3(CO)_{10}(\mu\text{-}CO)]^{2-}$ unit. In addition, there is a very weak mercurophilic contact, as indicated by the long Hg(1)···Hg(2) distance [3.684(3) Å] and the Hg(1)-Ru(1)-Hg(2) angle [86.38(8) °]. The structure of **4** is quite similar to that previously reported for *cis*-$[Os(CO)_4\{(\mu\text{-}Hg)Os_3(CO)_{10}(\mu\text{-}Cl)\}_2]$ [55].

The cluster **4** is electron poor possessing 134 CVE [7×8 (7Ru) + 2×12 (2Hg) + 26×2 (26CO) + 2 (charge)]. Indeed, the EAN rule would predict 136 CVE for a cluster composed of nine metal atoms and displaying 13 M-M bonds. This is rather surprising, since the Hg(1)···Hg(2) contact is almost non-bonding and this would increase the expected electron count from 136 to 138 CVE. A possible explanation is the fact that d^{10} Hg(II) ions may not reach 18 valence electrons, especially when their coordination number is lower than four.

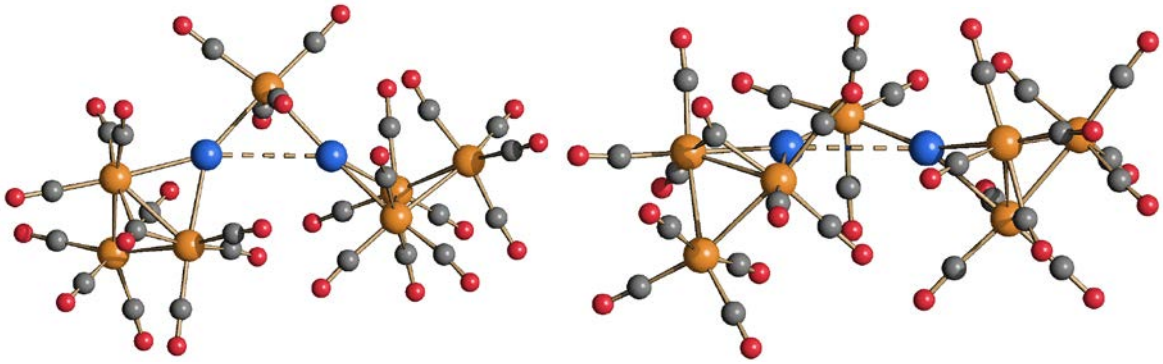

Fig. 3. Two views of the molecular structure of **4** (orange Ru; blue Hg; red O; grey C).

Table 2. Main bond distances (Å) and angles (°) of **4**. Cotton's formal shortness ratios (FSR) are reported in parentheses [74]. Pauling's atomic radii employed [75]: Ru 1.241 Å, Hg 1.440 Å. See Scheme 3 for labeling.

Hg(1)···Hg(2)	3.684(3) *(1.28)*		
Hg(1)-Ru(1)	2.706(3) *(1.01)*	Hg(2)-Ru(1)	2.677(3) *(1.00)*
Hg(1)-Ru(2)	2.764(3) *(1.03)*	Hg(1)-Ru(3)	2.809(3) *(1.05)*
Hg(2)-Ru(5)	2.797(3) *(1.04)*	Hg(2)-Ru(6)	2.752(3) *(1.03)*
Ru(2)-Ru(3)	2.859(3) *(1.15)*	Ru(5)-Ru(6)	2.890(4) *(1.16)*
Ru(2)-Ru(4)	2.879(3) *(1.16)*	Ru(5)-Ru(7)	2.847(4) *(1.15)*
Ru(3)-Ru(4)	2.853(4) *(1.15)*	Ru(6)-Ru(7)	2.855(4) *(1.15)*
$Ru\text{-}CO_{terminal}^{range}$	1.89(4)-1.98(3)	$Ru\text{-}CO_{terminal}^{average}$	1.93(15)
Ru(2)-C(1)	2.05(3)	Ru(3)-C(1)	2.11(3)
Ru(5)-C(2)	2.10(3)	Ru(6)-C(2)	2.10(3)
Hg(1)-Ru(1)-Hg(2)	86.38(8)		
Ru(2)-Hg(1)-Ru(3)	61.72(7)	Ru(5)-Hg(2)-Ru(6)	62.78(8)
Ru(2)-C(1)-O(1)	140(3)	Ru(3)-C(1)-O(1)	133(3)
Ru(5)-C(2)-O(2)	136(3)	Ru(6)-C(2)-O(2)	136(3)
$\alpha_{CO(1)}$	0.03(4)	$\alpha_{CO(2)}$	0.00(4)

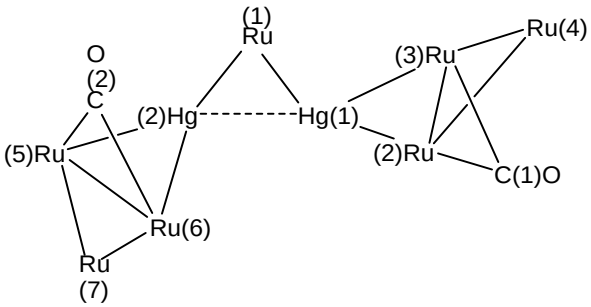

Scheme 3. Labeling of **4**.

The RSMD between computed and experimental geometries of **4** is quite low, 0.328 Å. As deducible from Figure 4 and Table S2, the Hg centers form stronger Hg-Ru interactions with the {$Ru(CO)_4$} fragment with respect to the {$Ru_3(CO)_{10}(\mu\text{-}CO)$} units. On the basis of the computed data, Hg(1)-Ru(1) and Hg(2)-Ru(1) bonds are stronger than the Hg-Ru interactions in compound **3**. The ρ and V values for the other Hg-Ru b.c.p.'s in **4** are similar to those obtained for **3**. As for compound **3**, also for **4** the AIM analysis was unable to localize (3,-1) b.c.p. between Ru centers bridged by CO.

No Hg⋯Hg b.c.p. was found, and accordingly the gradient of the electron density never goes to zero along the Hg⋯Hg path, as shown in Figure S5 in the Supporting Information. Moreover, no ring critical point (r.c.p.) related to the Hg(1)-Hg(2)-Ru(1) triangle was localized. Such a behavior is in line with what previously observed for isoelectronic $d^{10}\cdots d^{10}$ interactions in *cis*-$Fe(CO)_4\{M(NHC)\}_2$ (M = Cu, Ag, Au; NHC = N-heterocyclic carbene) complexes [21,24]. The weak mercurophilic contact in **4** appears therefore limited to a non-localized dispersion interaction, too weak to be computationally investigated by means of AIM analysis.

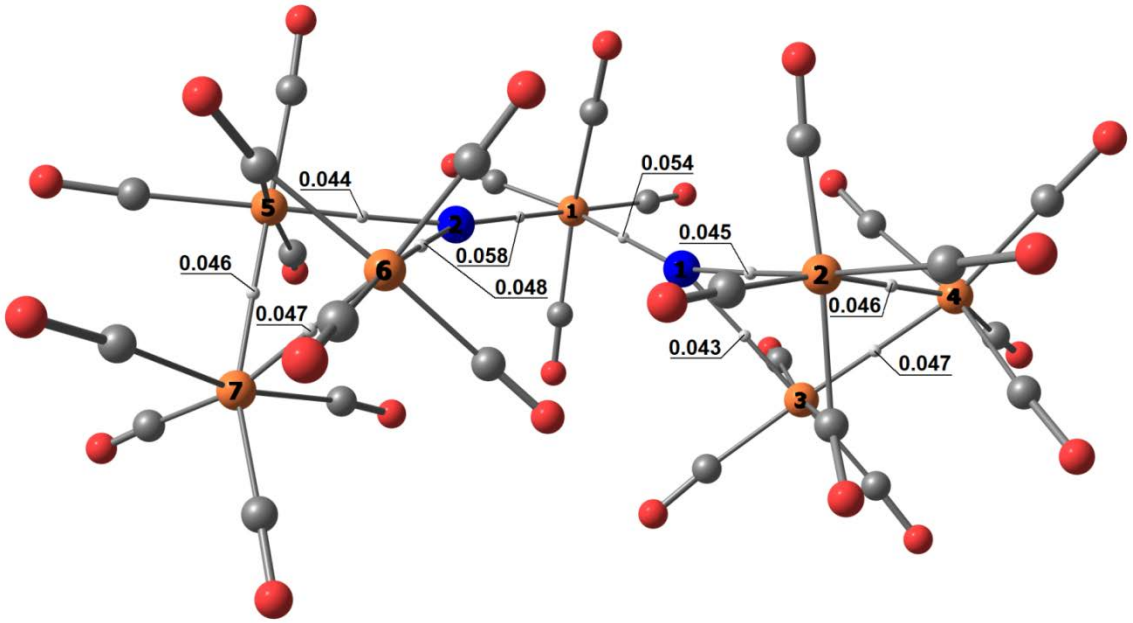

Fig. 4. DFT-optimized structure of **4** (orange Ru; blue Hg; red O; grey C) with localized M-M (3,-1) b.c.p.'s (white) and corresponding electron density values in a.u.

2.2.3 $[Hg_3Ru_8(CO)_{30}]^{2-}$ (5)

The solid state structure of $[NEt_4]_2$[**5**] consists of an ionic packing of $[NEt_4]^+$ cations and **5** anions. The cluster anion may be viewed as composed of a linear $[Hg_3]^{6+}$ core bonded to two bridging $[Ru(CO)_4]^{2-}$ and two $[Ru_3(CO)_{10}(\mu\text{-}CO)]^{2-}$ units (Figure 5 and Table 3). The central Hg(1) atom is located on an inversion centre and, therefore, only half of the molecule is independent. The Hg(1)···Hg(2) contact [3.1776(7) Å] of **5** is significantly shorter than that of **4**, suggesting a stronger mercurophilic interaction. Such contact is comparable to that recently found in porphyrin complexes containing a linear $[Hg_3]^{6+}$ unit [18].

As in the case of **4**, also **5** is electron poor possessing 162 CVE [8×8 (8Ru) + 3×12 (3Hg) + 30×2 (30CO) + 2 (charge)]. Indeed, considering 11 metal atoms and 16 M-M bonds, the expected electron count would have been 166 CVE. This is somehow in keeping with the fact the Hg(II) centers display low coordination numbers, that is two for Hg(1), and three for Hg(2) and Hg(2A) (considering only Hg-Ru bonds).

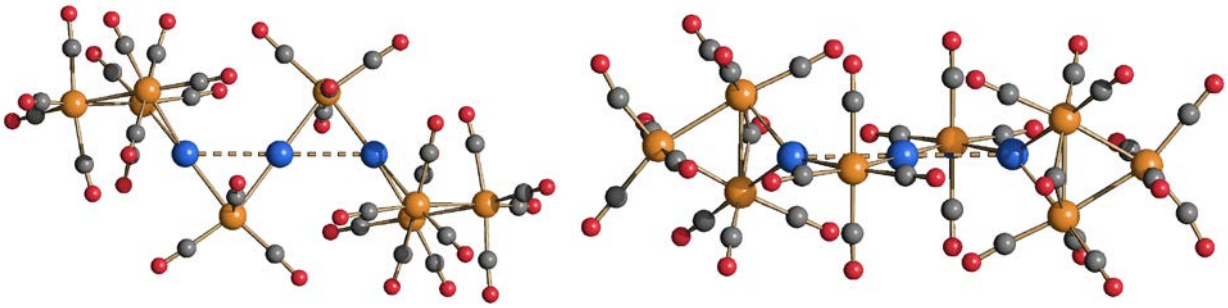

Fig. 5. Two views of the molecular structure of **5** (orange Ru; blue Hg; red O; grey C).

Table 3. Main bond distances (Å) and angles (°) of **5**. Cotton's formal shortness ratios (FSR) are reported in parentheses [74]. Pauling's atomic radii employed [75]: Ru 1.241 Å, Hg 1.440 Å. See Scheme 4 for labeling.

Hg(1)···Hg(2)	3.1776(7) *(1.10)*	Hg(1)-Ru(1)	2.6726(13) *(1.00)*
Hg(2)-Ru(1)	2.6783(12) *(1.00)*	Hg(2)-Ru(2)	2.7756(12) *(1.04)*
Hg(2)-Ru(3)	2.7634(12) *(1.03)*	Ru(2)-Ru(3)	2.8765(15) *(1.16)*
Ru(2)-Ru(4)	2.8304(16) *(1.14)*	Ru(3)-Ru(4)	2.8448(17) *(1.15)*
$Ru\text{-}CO_{terminal}^{range}$	1.891(16)-1.959(17)	$Ru\text{-}CO_{terminal}^{average}$	1.92(6)
Ru(2)-C(1)	2.106(14)	Ru(3)-C(1)	2.088(13)
Hg(2)-Hg(1)-Hg(2A)	180.0	Hg(1)-Ru(1)-Hg(2)	72.86(3)
Ru(2)-Hg(2)-Ru(3)	62.57(3)	Ru(1)-Hg(1)-Ru(1A)	180.0
Ru(2)-C(1)-O(1)	134.6(10)	Ru(3)-C(1)-O(1)	138.6(11)
$\alpha_{CO(1)}$	0.009(19)	Mean deviation from least-square plane Hg(1)-Hg(2)-Hg(2A)-Ru(1)-Ru(1A)	0.0000

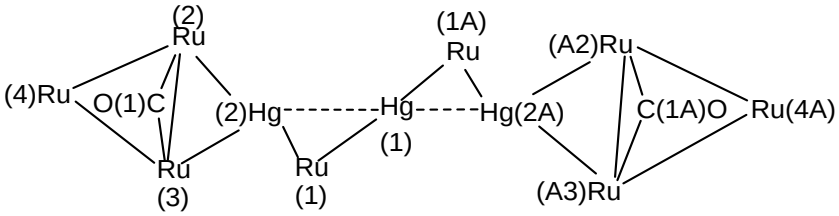

Scheme 4. Labeling of $[Hg_3Ru_8(CO)_{30}]^{2-}$.

The DFT-optimized structure of **5** (Figure 6) agrees with the X-ray data (RSMD = 0.224 Å) and the presence of an inversion centre was appreciably maintained by the simulation (R = 0.002 for the C_i point group). The AIM data (Table S3 in the Supporting Information) confirm the symmetry of compound **5**. The computed average Hg···Hg distance is 3.300 Å, about 3% longer than the experimental value despite the presence of corrections for the dispersion interactions in the DFT method used (see the Experimental section). The slight overestimation of the Hg···Hg distances is probably related to the known weakness of DFT methods in predicting closed-shell dispersion interactions [80]. The Hg···Hg distances in **5** are however much shorter than the value computed for **4**, 3.694 Å. Despite this outcome, the AIM analysis was unable to localize (3,-1) b.c.p.'s between the Hg centers or (3,+1) r.c.p. related to the Ru(1)-Hg(1)-Hg(2) and Ru(1A)-Hg(1)-Hg(2A) triangles. Such a result is comparable with that obtained for the Au(I)···Au(I) interactions in $[Au_3\{Fe(CO)_4\}_2(PPh_3)_2]^-$ [22].

Two Hg-Ru (3,-1) b.c.p.'s were localized for the central Hg and three Hg-Ru b.c.p.'s for the other Hg centers. As for **4**, also in **5** the Hg-$\{Ru(CO)_4\}$ bonds are stronger than the Hg-$\{Ru_3(CO)_{10}(\mu\text{-}CO)\}$ ones. The lack of localized Hg(1)···Hg(2/2A) interactions and the presence of Hg-Ru(1/1A) bonds is confirmed by the comparison of the gradients of electron density along the Hg(2)···Hg(2A) and Ru(1)···Ru(1A) paths, shown in Figure S6 in the Supporting Information. The three Hg centers have similar Hirshfeld charges, 0.106 a.u. for Hg(1) and 0.083 for Hg(2/2A), this indicating that the formal oxidation state is the same. Two Ru-Ru b.c.p.'s were found for each $\{Ru_3\}$ triangle, since no b.c.p. was localized between the Ru centers connected by the bridging carbonyl ligands.

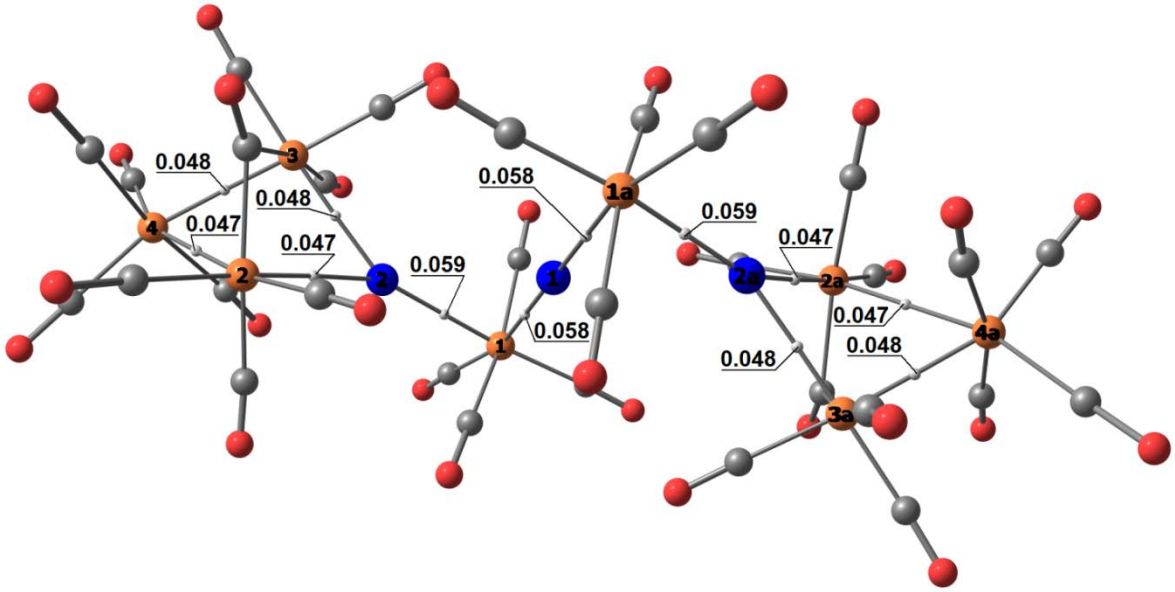

Fig. 6.. DFT-optimized structure of **5** (orange Ru; blue Hg; red O; grey C) with localized M-M (3,-1) b.c.p.'s (white) and corresponding electron density values in a.u.

2.2.4 $[Hg_4Ru_{10}(CO)_{32}]^{4-}$ (6)

The anion **6** may be viewed as composed of a $[Hg_4]^{8+}$ distorted rectangle (rhombus) whose short edges are bonded to two $[Ru_4(CO)_{10}(\mu\text{-}CO)_2]^{4-}$ tetrahedra, whereas the longer edges are bridged by two $[Ru(CO)_4]^{2-}$ units (Figure 7 and Table 4). Hg(1) is capping one triangular face of the Ru_4 tetrahedron, whereas Hg(2) is bonded to one edge of the same triangular face. This results in a $HgRu_4$ trigonal bipyramid, whose Hg(1)Ru(1)Ru(2) face is capped by Hg(2).

The shortest Hg-Ru distances are those involving the $[Ru(CO)_4]^{2-}$ units [Hg(1)-Ru(5A) 2.7134(11) Å, FSR 1.01; Hg(2)-Ru(5) 2.6957(10) Å, FSR 1.01], whereas the longest ones are those of the Hg(1)Ru(1)Ru(2) face capped by Hg(2) [Hg(1)-Ru(1) 2.8618(10) Å, FSR 1.07; Hg(1)-Ru(2) 2.9079(10) Å, FSR 1.08]. The remaining three Hg-Ru contacts display intermediate distances [Hg(1)-Ru(4) 2.7806(10) Å, FSR 1.04; Hg(2)-Ru(1) 2.7706(10) Å, FSR 1.03; Hg(2)-Ru(2) 2.7782(10) Å, FSR 1.04].

The Hg(1)···Hg(2) [3.4350(7) Å, FSR 1.19] and Hg(1)···Hg(2A) [3.5120(7) Å, FSR 1.22] contacts suggest the presence of weak mercurophilic interactions.

The molecular structure of the free $[Ru_4(CO)_{12}]^{4-}$ tetra-anion is unknown, whereas the related hydrides $[H_{4-n}Ru_4(CO)_{12}]^{n-}$ (n = 0-3) have been structurally characterized [81,82]. The two $[Ru_4(CO)_{12}]^{4-}$ units of **6** contain ten terminal and two semi-bridging [α = 0.23 and 0.38] CO ligands.

It must be remarked that there are only limited examples of structurally characterized carbonyl clusters containing a Hg_4 core, that is $Hg_4Mn_4(CH_3C_5H_4)_4(CO)_8$ [64], $Hg_4Fe_4(L)_2(CO)_{12}$ (L = 2,6-bis(disphenylphosphino)pyridine) [67], $Hg_4Re_4(Cp)_4(CO)_8$ [83] and $Hg_4Ru_4(CO)_{16}$ [63].

At difference with **4** and **5**, **6** is electron rich possessing 196 CVE [10×8 (10Ru) + 4×12 (4Hg) + 32×2 (32CO) + 4 (charge)] instead of 192 CVE as predicted by the EAN rule (14 metal atoms and 30 M-M bonds, considering also the Hg-Hg contacts). In this case, the extra-electrons would somehow compensate the very weak Hg···Hg interactions. Moreover, Hg(1) and Hg(1A) are tetra-coordinated, whereas Hg(2) and Hg(2A) display only three Ru-Hg contacts. Conversely, the electron poor clusters **4** and **5** contain only Hg centers with coordination numbers three or two.

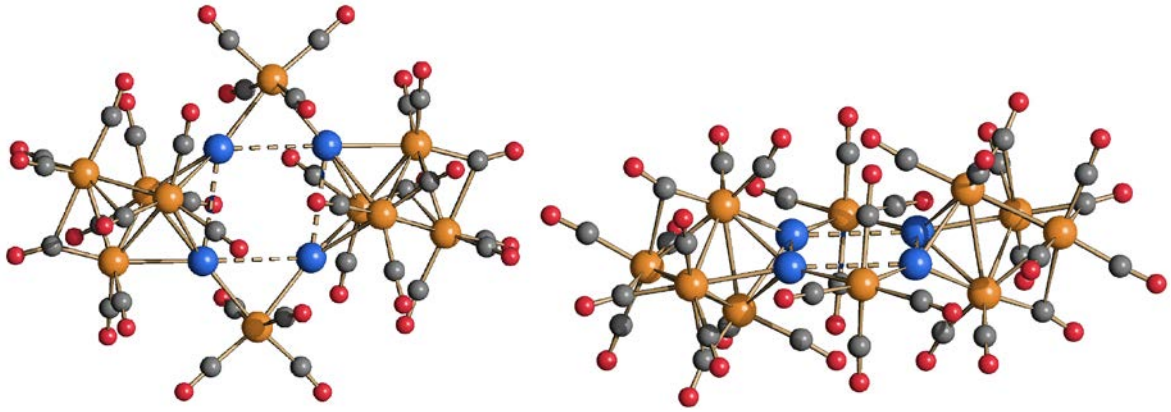

Fig. 7. Two views of the molecular structure of **6** (orange Ru; blue Hg; red O; grey C).

Table 4. Main bond distances (Å) and angles (°) of **6**. Cotton's formal shortness ratios (FSR) are reported in parentheses [74]. Pauling's atomic radii employed [75]: Ru 1.241 Å, Hg 1.440 Å. See Scheme 5 for labeling.

Hg(1)···Hg(2)	3.4350(7) *(1.19)*	Hg(1)···Hg(2A)	3.5120(7) *(1.22)*
Hg(1)-Ru(5A)	2.7134(11) *(1.01)*	Hg(2)-Ru(5)	2.6957(10) *(1.01)*
Hg(1)-Ru(1)	2.8618(10) *(1.07)*	Hg(1)-Ru(2)	2.9079(10) *(1.08)*
Hg(1)-Ru(4)	2.7806(10) *(1.04)*	Hg(2)-Ru(1)	2.7706(10) *(1.03)*
Hg(2)-Ru(2)	2.7782(10) *(1.04)*		
Ru(1)-Ru(2)	3.0136(12) *(1.21)*	Ru(1)-Ru(3)	2.8312(13) *(1.14)*
Ru(1)-Ru(4)	2.8412(13) *(1.14)*	Ru(2)-Ru(3)	2.8280(13) *(1.14)*
Ru(2)-Ru(4)	2.8834(13) *(1.16)*	Ru(3)-Ru(4)	2.8417(13) *(1.14)*
$Ru\text{-}CO_{terminal}^{range}$	1.868(12)-1.962(16)	$Ru\text{-}CO_{terminal}^{average}$	1.90(4)
Ru(1)-C(1)	1.898(13)	Ru(4)-C(3)	2.617(2)
Ru(3)-C(2)	2.404(12)	Ru(4)-C(2)	1.953(13)
Hg(2)-Hg(1)-Hg(2A)	81.66(2)	Hg(1)-Hg(2)-Hg(1A)	98.34(2)
Hg(1A)-Ru(5)-Hg(2)	81.00(3)	Mean deviation from least-square plane Hg(1)-Hg(2)-Hg(1A)-	0.004

		Hg(2A)-Ru(5)-Ru(5A)	
Ru(1)-C(1)-O(1)	160.5(10)	Ru(4)-C(1)-O(1)	123.3(10)
Ru(3)-C(2)-O(2)	128.0(9)	Ru(4)-C(2)-O(2)	151.2(10)
$\alpha_{CO(1)}$	0.38	$\alpha_{CO(2)}$	0.23

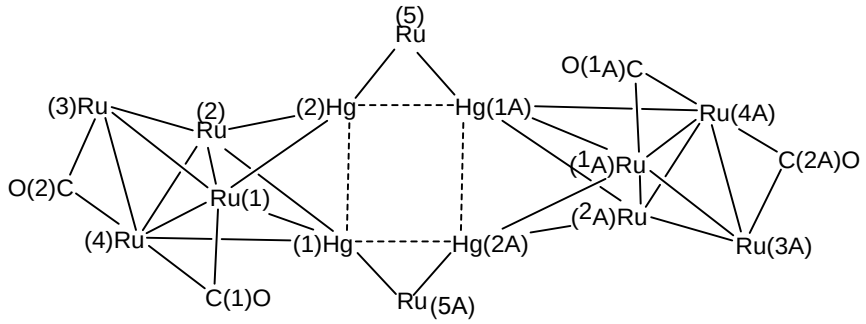

Scheme 5. Labeling of **6**.

The experimentally observed symmetry of **6** was not precisely maintained during the computational optimization of the cluster (R = 0.314 with respect to the C_i point group). The RMSD between experimental and computed data is however quite low, 0.383 Å, and the same numbering shown in Scheme 5 was maintained for clarity. Moreover, the analysis of the electron density did not highlight meaningful differences between the two halves of **6**. As for the previously discussed clusters, the AIM analysis (Figure 8 and Table S4 in the Supporting Information) did not localize (3,-1) b.c.p. between the Hg atoms. On the other hand, one r.c.p. at the centre of the $\{Hg_4\}$ was found, with very low ρ value (0.0015 a.u.) and V value close to zero (-0.0005 a.u.). The situation is qualitatively comparable with that found in square clusters of coinage metals having general formula $[\{MFe(CO)_4\}_4]^{4-}$ (M = Cu, Ag, Au) [25]. These data, combined with the low, positive values of E (0.0002 a.u.) and $\nabla^2\rho$ (0.0039 a.u.), suggest that the interactions among the Hg centers are of van der Waals type [78]. The presence of the r.c.p. and the lack of Hg···Hg b.c.p. was also confirmed by the trends of the gradient of electron density along the Hg···Hg paths, shown in Figure S7 in the Supporting Information.

For further comparison, the AIM analysis was extended to the neutral tetramers $Hg_4Fe_4(CO)_{16}$ [65] and $Cd_4Fe_4(CO)_{16}$ [66]. The expected Fe-Hg and Fe-Cd (3,-1) b.c.p.'s were localized, but no Cd···Cd or Hg···Hg b.c.p., an outcome confirmed by the gradient of electron density along the M···M paths. As for compound **6**, one (3,+1) r.c.p. is present at the centre of the $\{Cd_4\}$ and $\{Hg_4\}$ fragments (see Figure S8 in the Supporting Information). The ρ and V values for $Hg_4Fe_4(CO)_{16}$ are respectively 0.0020 a.u. and -0.0007 a.u., and the E and $\nabla^2\rho$ values are small and positive (0.0003 a.u. and 0.0052 a.u., respectively). Values in line with $Hg_4Fe_4(CO)_{16}$ were obtained

for the analogous cadmium derivative $Cd_4Fe_4(CO)_{16}$ (ρ =0.0019 a.u., V = -0.0004 a.u., E = 0.0004 a.u., $\nabla^2\rho$ = 0.0048 a.u.). The Hg···Hg closed-shell interactions in **6** appear therefore qualitatively comparable to those present in $Hg_4Fe_4(CO)_{16}$ [65].

Accordingly to the localization of the (3,-1) b.c.p. in compound **6**, four Hg-Ru bonds are formed by Hg(1) and Hg(1A) and three by Hg(2) and Hg(2A). The values reported in Table S4 indicate that the strongest interactions occur with Ru(5) and Ru(5A), as already deduced from the structural data. The other Hg-Ru b.c.p.'s have quite comparable ρ and V values, with the Hg(2/2A)-Ru(1/1A) and Hg(1/1A)-Ru(4/4A) interactions slightly stronger than Hg(1/1A)-Ru(1/1A), Hg(1/1A)-Ru(2/2A) and Hg(1/1A)-Ru(2/2A). For what concerns the Ru-Ru interactions, (3,-1)-b.c.p.'s were not localized between Ru(3/3A) and Ru(4/4A), in line with the previous results concerning Ru centers connected by μ-CO ligands. On the other hand, Ru-Ru b.c.p.'s are present between Ru(1/1A) and Ru(4/4A), probably because of the semi-bridging coordination mode of CO. The weakest Ru-Ru bonds are Ru(1/1A)-Ru(2/2A), a result attributable to the donation of electron density to the Hg centers.

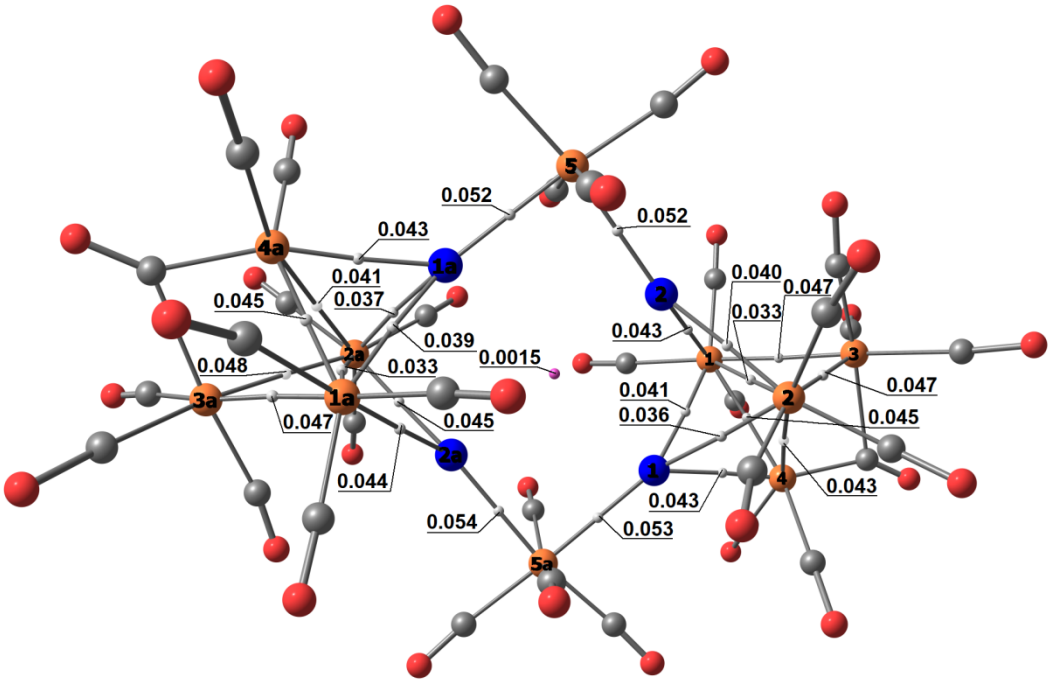

Fig. 8 DFT-optimized structure of **6** (orange Ru; blue Hg; red O; grey C) with localized M-M (3,-1) b.c.p.'s (white) and {Hg_4} (3,+1) r.c.p. (pink) and corresponding electron density values in a.u.

2.2.5 $[Ru_3(CO)_{10}(CH_3COO)]^-$ (7)

The molecular structure of **7** is composed of a triangular $Ru_3(CO)_7(\mu\text{-}CO)_3$ unit with a bridging CH_3COO^- ligand (Figure 9 and Table 5). The Ru(2)-Ru(3) edge [2.7527(2) Å] bridged by both a μ-CO and the acetate is significantly shorter than Ru(1)-Ru(2) [2.8560(2) Å] and Ru(1)-Ru(3)

[2.8503(2) Å] supported only by a μ-CO ligand. The asymmetry parameter for the three μ-CO ligands is in the typical range for symmetric edge bridging carbonyls, even though it is almost zero for CO(3) [$\alpha_{CO(3)}$ = 0.005(3)] whereas it is sensibly greater for CO(1) and CO(2) [$\alpha_{CO(1)}$ = 0.034(3), $\alpha_{CO(2)}$ = 0.040(3)]. This is likely to be due to the fact that Ru(2) and Ru(3) are bonded to the acetate ligand which is a stronger base than the terminal carbonyls bonded to Ru(1). As a consequence, the π-back donation from Ru(2) and Ru(3) towards the μ-CO ligands is slightly greater than that of Ru(1). Indeed, Ru(3)-C(1) [2.098(2) Å] and Ru(2)-C(2) [2.103(2) Å] are slightly shorter that Ru(1)-C(1) [2.170(2) Å] and Ru(1)-C(2) [2.187(2) Å]. Coordination of an acetate ion to metal carbonyl clusters is rather rare and, in the case of triangular clusters, is limited to a few Os_3 carbonyls [84,85].

The cluster **7** possesses 48 CVE [3×8 (3Ru) + 10×2 (10CO) + 1×3 (1μ-CH_3COO) + 1 (charge)] as expected for a triangular cluster.

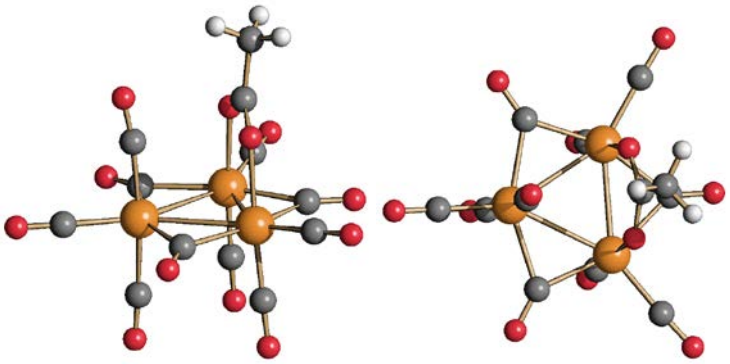

Fig. 9. Two views of the molecular structure of **7** (orange Ru; red O; grey C; white H).

Table 5. Main bond distances (Å) and angles (°) of **7**. Cotton's formal shortness ratios (FSR) are reported in parentheses [74]. Pauling's atomic radii employed [75]: Ru 1.241 Å. See Scheme 6 for labeling.

Ru(1)-Ru(2)	2.8560(2) *(1.15)*	Ru(1)-Ru(3)	2.8503(2) *(1.15)*
Ru(2)-Ru(3)	2.7527(2) *(1.11)*		
Ru(2)-O(11)	2.1561(14)	Ru(3)-O(12)	2.1481(14)
$Ru\text{-}CO_{terminal}^{range}$	1.849(2)-1.954(2)	$Ru\text{-}CO_{terminal}^{average}$	1.899(5)
Ru(1)-C(1)	2.170(2)	Ru(3)-C(1)	2.098(2)
Ru(1)-C(2)	2.187(2)	Ru(2)-C(2)	2.103(2)
Ru(2)-C(3)	2.131(2)	Ru(3)-C(3)	2.120(2)
C(11)-O(11)	1.260(3)	C(11)-O(12)	1.265(3)

Ru(2)-Ru(1)-Ru(3)	57.684(6)	Ru(1)-Ru(2)-Ru(3)	61.054(6)
Ru(2)-Ru(3)-Ru(1)	61.262(6)	O(11)-C(11)-O(12)	125.49(19)
Ru(2)-O(11)-C(11)	123.24(13)	Ru(3)-O(12)-C(11)	124.04(13)
Ru(1)-C(1)-O(1)	134.38(17)	Ru(3)-C(1)-O(1)	141.65(18)
Ru(1)-C(2)-O(2)	134.27(18)	Ru(2)-C(2)-O(2)	141.53(18)
Ru(2)-C(3)-O(3)	139.63(17)	Ru(3)-C(3)-O(3)	139.58(17)
$\alpha_{CO(1)}$	0.034(3)	$\alpha_{CO(2)}$	0.040(3)
$\alpha_{CO(3)}$	0.005(3)		

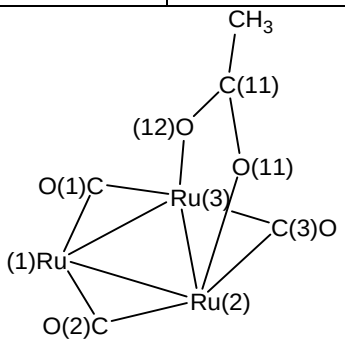

Scheme 6. Labeling of **7**.

2.2.6 $[Ru_2Cl_4(CO)_5]^{2-}$ (8)

The molecular structure of **8** is composed of a $[Ru_2(\mu\text{-}Cl)(\mu\text{-}CO)]^+$ core with one Cl^- and two CO ligands bonded to Ru(1), and two Cl^- and two CO ligands bonded to Ru(2), all in a terminal mode (Figure 10 and Table 6). Therefore, considering also the bridging ligands and excluding the Ru(1)-Ru(2) contact, Ru(1) displays a square-pyramidal coordination whereas Ru(2) shows an octahedral coordination. The cluster possesses 34 CVE [2×8 (2Ru) + 5×2 (5CO) + 3×1 (3Cl) + 1×3 (1μ-Cl) + 2 (charge)] as expected for a M-M bonded dimer. Indeed, the Ru(1)-Ru(2) distance [3.1344(6) Å], even if slightly elongated, is in the typical range for Ru-Ru bonds. In addition, a weak inter-molecular Ru(1)⋯Ru(1A) contact [3.947(2) Å] is present in the solid state, probably due to the fact that Ru(1) is coordinatively unsaturated compared to Ru(2). This generates weakly interacting $\{[Ru_2Cl_4(CO)_5]_2\}^{4-}$ dimers within the crystalline structure.

Starting from the DFT-optimized structure of $[Ru_2Cl_4(CO)_5]^{2-}$ (computed Ru(1)-Ru(2) distance of 3.129 Å in gas phase and 3.120 Å in the presence of continuous medium), the first attempt to simulate the corresponding $\{[Ru_2Cl_4(CO)_5]_2\}^{4-}$ dimer in gas phase failed, probably because of the repulsive electrostatic interactions between the $[Ru_2Cl_4(CO)_5]^{2-}$ units, with Ru(1)⋯Ru(1A) distance at the stationary point around 6 Å. The problem was solved with the introduction of implicit solvation, with computed Ru(1)⋯Ru(1A) distance of 3.430 Å. The AIM analysis was able to find a (3,-1) b.c.p. between Ru(1) and Ru(1A) characterized by quite low

electron density (ρ = 0.015 a.u.). The other parameters (V = -0.009 a.u., E = -0.001 a.u. and $\nabla^2\rho$ = 0.025 a.u.) however agree with the presence of a weak metal-metal interaction. The DFT-optimized structure of $\{[Ru_2Cl_4(CO)_5]_2\}^{4-}$ with the Ru(1)···Ru(1A) b.c.p. is shown in Figure S9 in the Supporting Information. The Ru(1)···Ru(1A) overlap is mainly attributable to the HOMO-1 molecular orbital, but the interaction is weakened by the antibonding character of the HOMO (see Figure S10 in the Supporting Information). However, the two contributions do not completely cancel each other, as deductible from the electron density plot in Figure S10 in the Supporting Information.

The di-anion **8** is formally related to $[Ru_2Cl_4(CO)_6]$, which contains two μ-Cl ligands, two terminal chlorides and six terminal carbonyls [86]. Indeed, the replacement of one CO with two electrons formally transforms $[Ru_2Cl_4(CO)_6]$ into **8**. It must be remarked that, due to the different stereochemistry of the ligands, $[Ru_2Cl_4(CO)_6]$ possesses 36 CVE [2×8 (2Ru) + 6×2 (6CO) + 2×1 (2Cl) + 2×3 (2μ-Cl)] instead of 34 CVE for **8**. As a consequence, the former neutral cluster does not contain a direct Ru-Ru bond [*ca.* 3.6 Å], whereas a direct bond is present in **8** [3.1344(6) Å]. This is in keeping with the fact that the formal oxidation state of the two Ru centers in 2+ in $[Ru_2Cl_4(CO)_6]$ and +1 in **8**.

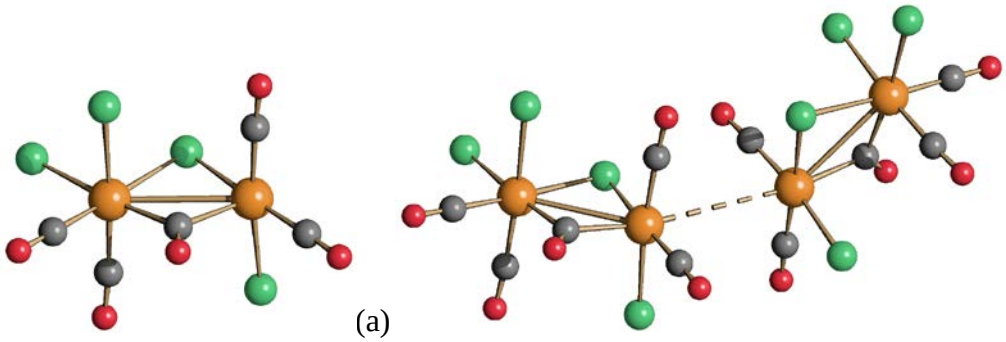

Fig. 10. (a) Molecular structure of **8** and (b) the $\{[Ru_2Cl_4(CO)_5]_2\}^{4-}$ dimer resulting from the long Ru···Ru contact [3.947(2) Å] (orange Ru; green Cl; red O; grey C).

Table 6. Main bond distances (Å) and angles (°) of **8**. Cotton's formal shortness ratios (FSR) are reported in parentheses [71]. Pauling's atomic radii employed [72]: Ru 1.241 Å, Cl 0.994 Å. See Scheme 9 for labeling.

Ru(1)-Ru(2)	3.1344(6) *(1.26)*	Ru(1)···Ru(1A)	3.947(2) *(1.59)*
Ru(1)-Cl(1)	2.4530(15) *(1.10)*	Ru(2)-Cl(1)	2.4953(14) *(1.12)*
Ru(1)-Cl(2)	2.4157(14)		

	(1.08)		
Ru(2)-Cl(3)	2.4381(13) *(1.09)*	Ru(2)-Cl(4)	2.5021(17) *(1.12)*
Ru(1)-C(1)	2.035(6)	Ru(2)-C(1)	2.054(5)
Ru(1)-C(2)	1.837(7)	Ru(1)-C(3)	1.856(6)
Ru(2)-C(4)	1.868(6)	Ru(2)-C(5)	1.856(6)
Ru(1)-C(1)-Ru(2)	100.1(3)	Ru(1)-Cl(1)-Ru(2)	78.60(4)
Cl(2)-Ru(1)-C(3)	173.26(18)	C(2)-Ru(1)-Cl(1)	174.5(2)
Cl(3)-Ru(2)-C(4)	175.9(2)	Cl(4)-Ru(2)-C(1)	
C(5)-Ru(2)-Cl(1)	174.81(18)	Ru(2)-Ru(1)⋯Ru(1A)	137.1(3)
$\alpha_{CO(1)}$	0.009(8)	$\alpha_{Cl(1)}$	0.017(2)
Mean deviation from the Ru(1)Ru(2)C(1)Cl(1) least square plane	0.292		

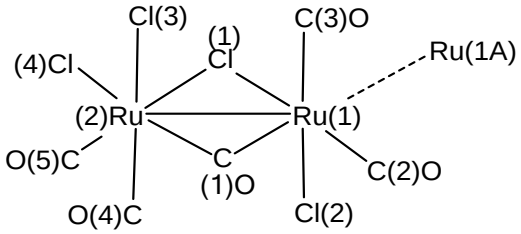

Scheme 9. Labeling of **8**. The weak contact to Ru(1A) within the dimer is represented with a dashed line.

3. Conclusions

Four new heterometallic Ru-Hg carbonyl clusters **3-6** have been prepared and structurally characterized by SC-XRD. These contain $[Hg]^{2+}$, $[Hg_2]^{4+}$, $[Hg_3]^{6+}$, and $[Hg_4]^{8+}$ cores stabilized by $[Ru(CO)_4]^{2-}$, $[Ru_3CO)_{11}]^{2-}$ and $[Ru_4(CO)_{12}]^{4-}$ fragments. Thus, **3-6** may be viewed as Hg(II) complexes displaying metal carbonyl anions as ligands. Mercurophilic Hg(II)⋯Hg(II) contacts are present within the $[Hg_2]^{4+}$, $[Hg_3]^{6+}$, and $[Hg_4]^{8+}$ cores, most likely based on poorly localized dispersion interactions rather than on genuine covalent bonds. The lack of localization of Hg⋯Hg (3,-1) bond critical points is in agreement with this picture, but unfortunately does not allow an insight into the nature of the interactions in **4** and **5** by means of AIM analysis. More information was obtained from the ring critical point of compound **6**, that indicated the presence of closed-shell $d^{10}\cdots d^{10}$ interactions comparable to those observed for isoelectronic $\{M_4\}$ fragments in other tetrameric heterometallic clusters. The present findings corroborate the opinion that heterometallic

carbonyl clusters are well suited platforms for the experimental and theoretical investigation of weak metallophilic interactions [2,5,16,20-29].

4. Experimental

4.1 General procedures.

All reactions and sample manipulations were carried out using standard Schlenk techniques under nitrogen and in dried solvents. All the reagents were commercial products (Aldrich) of the highest purity available and used as received, except $[NEt_4][HRu_3(CO)_{11}]$ and $[NEt_4]_3[HRu_4(CO)_{12}]$, which has been prepared according to the literature [81]. Analyses of C, H and N were obtained with a Thermo Quest Flash EA 1112NC instrument. IR spectra were recorded on a Perkin Elmer Spectrum One interferometer in CaF_2 cells. Structure drawings have been performed with SCHAKAL99 [87].

4.2 Synthesis of $[NEt_4]_2[HgRu_6(CO)_{22}]$ ($[NEt_4]_2$[3])

$$[NEt_4][HRu_3(CO)_{11}] + Hg(CH_3CO_2) \xrightarrow[\text{r.t., 1h}]{CH_2Cl_2} [NEt_4]_2[HgRu_6(CO)_{22}]$$

Solid $Hg(CH_3CO_2)$ (0.057 g, 0.179 mmol, 0.35 eq) was added to a solution of $[NEt_4]$[**1**] (0.380 g, 0.520 mmol) in CH_2Cl_2 (15 mL). The mixture was stirred at room temperature for 1 h and, then, the solvent was removed in vacuum. The residue was washed with water (2×20 mL), toluene (2×10 mL), and then extracted with CH_2Cl_2 (15 mL). The dichloromethane solution was layered with n-pentane affording crystals of $[NEt_4]_2$[**3**] suitable for X-ray analysis (yield 86%).

$C_{38}H_{40}HgN_2O_{22}Ru_6$ (1683.73): calcd. (%): C 27.11, H 2.39, N 1.66; found: C 26.91, H 2.62, N 1.38. IR (CH_2Cl_2, 298 K) ν_{CO}: 2065(w), 2041(w), 2006(vs), 1980(sh), 1945(m) cm^{-1}. IR (Nujol, 298 K) ν_{CO}: 2055(w), 2004(s), 1988(vs), 1961(m), 1950(m), 1930(m) cm^{-1}.

4.3 Synthesis of $[NEt_4]_2[HgRu_6(CO)_{22}]$ ($[NEt_4]_2$[3]) and $[NEt_4]_2[Hg_2Ru_7(CO)_{26}]$ ($[NEt_4]_2$[4])

$$[NEt_4][HRu_3(CO)_{11}] + Hg(CH_3CO_2)_2 \xrightarrow[\text{r.t., 1h}]{CH_2Cl_2} [NEt_4]_2[HgRu_6(CO)_{22}] + [NEt_4]_2[Hg_2Ru_7(CO)_{26}]$$

Solid $Hg(CH_3CO_2)_2$ (0.071 g, 0.222 mmol, 0.5 eq.) was added to a solution of $[NEt_4]$[**1**] (0.330 g, 0.444 mmol) in CH_2Cl_2 (15 mL). The mixture was stirred at room temperature for 1 h and, then, the solvent was removed in vacuum. The residue was washed with water (2×20 mL), toluene (2×10 mL), and then extracted with CH_2Cl_2 (15 mL). The dichloromethane solution was layered with n-pentane affording a mixture (*ca.* 1 : 1) of crystals of $[NEt_4]_2$[**3**] and $[NEt_4]_2$[**4**]·$0.5CH_2Cl_2$ suitable for X-ray analysis (yield 74%). Moreover, few yellow crystals of $[NEt_4][Ru_3(CO)_{10}(CH_3COO)]$ **($[NEt_4]_2$[7])** suitable for X-ray crystallography were obtained as by-product of the reaction.

[NEt_4]$_2$[3]: IR (CH_2Cl_2, 298 K) ν_{CO}: 2065(w), 2041(w), 2006(vs), 1980(sh), 1945(m) cm^{-1}. IR (Nujol, 298 K) ν_{CO}: 2055(w), 2004(s), 1988(vs), 1961(m), 1950(m), 1930(m) cm^{-1}

[NEt_4]$_2$[4]: IR (CH_2Cl_2, 298 K) ν_{CO}: 2065(w), 2041(w), 2006(vs), 1980(sh), 1945(m) cm^{-1}. IR (Nujol, 298 K) ν_{CO}: 2062(w), 2043(w), 2001(vs), 1967(s), 1936(s), 1716(m), 1695(m) cm^{-1}

[NEt_4][7]: IR (CH_2Cl_2, 298 K) ν_{CO}: 2065(w), 2041(w), 2006(vs), 1980(sh), 1945 (m) cm^{-1}. IR (Nujol, 298 K) ν_{CO}: 2021(s), 1954(m), 1935(m), 1918(w), 1809(m), 1796(m) cm^{-1}.

NOTE: The formation of [NEt_4]$_2$[**3**] is favored by decreasing the amount of $Hg(CH_3CO_2)_2$ employed to 0.35 mole equivalents. Using 0.5 moles of $Hg(CH_3CO_2)_2$ per mole of [NEt_4][**1**] a 1:1 mixture of [NEt_4]$_2$[**3**] and [NEt_4]$_2$[**4**] is obtained. Further increasing the amount of $Hg(CH_3CO_2)_2$ to 0.75 equivalents seems to favors the formation of [NEt_4]$_2$[**4**] compared to [NEt_4]$_2$[**3**]. Nonetheless, at this point, also some [NEt_4]$_2$[**5**] is formed, which becomes the major product by employing one mole of $Hg(CH_3CO_2)_2$ per mole of [NEt_4][**1**].

4.4 Synthesis of [NEt_4]$_2$[$Hg_3Ru_8(CO)_{30}$] ([NEt_4]$_2$[5])

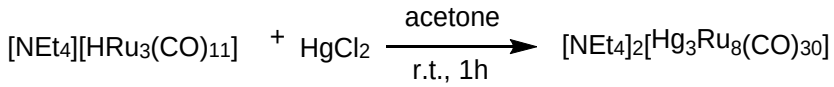

Solid $HgCl_2$ (0.128 g, 0.471 mmol) was added in two portions to a solution of [NEt_4][**1**] (0.350 g, 0.471 mmol) in acetone (15 mL). The mixture was stirred at room temperature for 1 h and, then, the solvent was removed in vacuum. The residue was washed with water (2×20 mL), toluene (2×10 mL), and then extracted with CH_2Cl_2 (15 mL)*. The dichloromethane solution was dried under reduced pressure and the solid dissolved in acetone. Crystals of [NEt_4]$_2$[**5**] suitable for X-ray analyses were obtained by layering n-hexane on the acetone solution (yield 63%).

$C_{46}H_{40}Hg_3N_2O_{30}Ru_8$ (2511.13): calcd. (%): C 22.00, H 1.61, N 1.12; found: C 22.24, H 1.88, N 0.79. IR (Acetone, 298 K) ν_{CO}: 2041(m), 2008(vs), 1972(sh), 1944(m) cm^{-1}. IR (Nujol, 298 K) ν_{CO}: 2045(w), 1999(s), 1975(vs), 1943(s), 1921(m) cm^{-1}.

NOTES: (a) The same product [NEt_4]$_2$[**5**] was obtained also performing the reaction in the same conditions under CO atmosphere. (b) By employing an excess of $HgCl_2$ (1.5 or 2 equivalents) the reaction led to the formation of crystals identified as [NEt_4][$Ru(CO)_3Cl_3$] ([NEt_4][**9**]) by X-ray analyses (comparison with data deposited within CSD). IR (CH_2Cl_2, 298 K) ν_{CO}: 2124(w), 2048(vs), 2031(sh) cm^{-1}. IR (Nujol, 298 K) ν_{CO}: 2120(w), 2046(s), 2035(s) 1727(m) cm^{-1}

* The residue not soluble in CH_2Cl_2 was extracted in CH_3CN and a few crystals of [NEt_4]$_2$[$Ru_2Cl_4(CO)_5$]·0.5CH_3CN ([NEt_4]$_2$[**8**]·0.5CH_3CN) were obtained by slow diffusion of n-hexane and di-iso-propyl-ether.

4.5 Synthesis of $[NEt_4]_4[Hg_4Ru_{10}(CO)_{30}]$ ($[NEt_4]_4$[6])

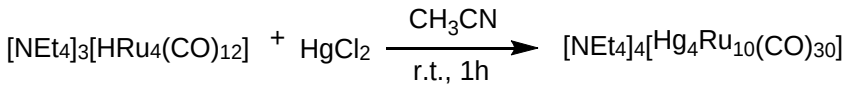

Solid $HgCl_2$ (0.0792 g, 0.292 mmol) was added in two portions to a solution of $[NEt_4]_3$[**2**] (0.330 g, 0.292 mmol) in CH_3CN (15 mL). The mixture was stirred at room temperature for 1 h and, then, the solvent was removed in vacuum. The residue was washed with water (2×20 mL), toluene (2×10 mL) and CH_2Cl_2 (2×10 mL),* dried under reduced pressure, and then extracted with acetone (15 mL). Crystals of $[NEt_4]_4$[**6**] suitable for X-ray analyses were obtained by layering n-hexane on the acetone solution (yield 67%).

$C_{64}H_{80}Hg_4N_4O_{32}Ru_{10}$ (3230.38): calcd. (%): C 23.80, H 2.50, N 1.73; found: C 23.46, H 2.21, N 1.98. IR (Acetone, 298 K) ν_{CO}: 2010 (s), 1974 (vs) cm^{-1}. IR (Nujol, 298 K) ν_{CO}: 2006 (m), 1964 (s) cm^{-1}.

* Crystals of $[NEt_4]$[**9**] were obtained by layering n-hexane on the dichloromethane solution. This product was identified by comparison with published data. In order to remove this by-product, the precipitate was washed many times with toluene and hexane and then dissolved in acetone.

4.6 X-ray Crystallographic Study.

Crystal data and collection details for $[NEt_4]_2$[**3**], $[NEt_4]_2$[**4**]·$0.5CH_2Cl_2$, $[NEt_4]_2$[**5**], $[NEt_4]_4$[**6**], $[NEt_4]$[**7**], $[NEt_4]_2$[**8**]·$0.5CH_3CN$ are reported in Table S5 in the Supporting Information. The diffraction experiments were carried out on a Bruker APEX II diffractometer equipped with a PHOTON2 detector using Mo–Kα radiation. Data were corrected for Lorentz polarization and absorption effects (empirical absorption correction SADABS) [88]. Structures were solved by direct methods and refined by full-matrix least-squares based on all data using F^2 [89]. Hydrogen atoms were fixed at calculated positions and refined by a riding model. All non-hydrogen atoms were refined with anisotropic displacement parameters. The crystals of $[NEt_4]_2$[**3**] and $[NEt_4]_2$[**4**]·$0.5CH_2Cl_2$ appeared to be non-merohedrally twinned. The TwinRotMat routine of PLATON was used to determine the twinning matrices and to write the reflection data file (.hkl) containing the twin components [90]. Refinement was performed using the instruction HKLF 5 in SHELXL and two BASF parameters, which refined as 0.258(5) and 0.50(4) for $[NEt_4]_2$[**3**] and $[NEt_4]_2$[**4**]·$0.5CH_2Cl_2$, respectively. Because of this twinning, the final *R* indices are slightly higher than for the other structures. In particular, the final R_1 ($I > 2\sigma(I)$) for $[NEt_4]_2$[**3**] is 0.1670. Despite this, the overall structure of **$[NEt_4]_2$[3]** is well established, and its geometry and bonding parameters quite reasonable and comparable to literature data. In addition, there is a perfect agreement between

the experimental (crystallographic) structure and the DFT optimized structure, further supporting the reliability of the crystal structure of **[NEt$_4$]$_2$[3]**.

4.7 Computational Details

Geometry optimizations were performed in gas phase using the PBEh-3c method, which is a reparametrized version of PBE0 [91] (with 42 % HF exchange) that uses a split-valence double-zeta basis set (def2-mSVP) with relativistic ECPs for Ru and Hg [92-94] and adds three corrections that consider dispersion, basis set superposition and other basis set incompleteness effects [95-97]. The "restricted" approach was used in all the cases. In selected cases the C-PCM solvation model was added, considering dichloromethane as continuous medium [98,99]. Calculations were performed with the ORCA software package, version 5.0.3 [100]. The output, converted in .molden format, was elaborated with the software Multiwfn, version 3.5 [101]. Cartesian coordinates of the DFT-optimized structures are provided in a separated .xyz file.

Appendix A. Supplementary material

Supplementary Information as .pdf file.

Cartesian coordinates of the DFT-optimized structures as a .xyz file.

CCDC 2184480 ([NEt$_4$]$_2$[**3**]), 2184481 ([NEt$_4$]$_2$[**4**]·0.5CH$_2$Cl$_2$), 2184482 ([NEt$_4$]$_2$[**5**]), 2184483 ([NEt$_4$]$_4$[**6**]), 2184484 ([NEt$_4$][**7**]), and 2184485 ([NEt$_4$]$_2$[**8**]·0.5CH$_3$CN) contain the supplementary crystallographic data for this paper. These data can be obtained free of charge from the Cambridge Crystallographic Data Centre.

Acknowledgements

We gratefully thank the University of Bologna for financial support. The authors thank the referees for useful suggestions in revising the manuscript.

Conflicts of Interest. The authors declare no conflict of interest.

References

[1] P. Pyykkö, Strong Closed-Shell Interactions in Inorganic Chemistry, Chem. Rev. 97 (1997) 597-636.

[2] S. Sculfort, P. Braunstein, Intramolecular d^{10}-d^{10} interactions in heterometallic clusters of the transition metals, Chem. Soc. Rev. 40 (2011) 2741-2760.

[3] H. Schmidbaur, A. Schier, Aurophilic interactions as a subject of current research: an up-date, Chem. Soc. Rev. 41 (2012) 370-412.

[4] Q. Zheng, S. Borsley, G. S. Nichol, F. Duarte, S. L. Cockroft, The Energetic Significance of Metallophilic Interactions, Angew. Chem. Int. Ed. 58 (2019) 12617-12623.

[5] P. Croizat, S. Sculfort, R. Welter, P. Braunstein, Hexa- and Octanuclear Heterometallic Clusters with Copper-, Silver-, or Gold-Molybdenum Bonds and d^{10}-d^{10} Interactions, Organometallics 35 (2016) 3949-3958.

[6] M. Olaru, J. F. Kögel, R. Aoki, R. Sakamoto, H. Nishihara, E. Lork, S. Mebs, M. Vogt, J. Beckmann, Tri- and Tetranuclear Metal-String Complexes with Metallophilic d^{10}-d^{10} Interactions, Chem. Eur. J. 26 (2020) 275-284.

[7] P. Pyykkö, J. Li, N. Runeberg, Predicted Ligand Dependence of the Au(I)···Au(I) Attraction in $(XAuPH_3)_2$, Chem. Phys. Lett. 218 (1994) 133-138.

[8] H. Schmidbaur, The Aurophilicity Phenomenon: A Decade of Experimental Findings, Theoretical Concepts and Emerging Applications, Gold. Bull. 33 (2000) 3-10.

[9] H. Schmidbaur, A. Schier, A briefing on aurophilicity, Chem. Soc. Rev. 37 (2008) 1931-1951.

[10] M. J. Katz, K. Sakai, D. B. Leznoff, The Use of Aurophilic and Other Metal-Metal Interactions as Crystal Engineering Design Elements to Increase Structural Dimensionality, Chem. Soc. Rev. 37 (2008) 1884-1895.

[11] P. Pyykkö, Theoretical chemistry of gold. III, Chem. Soc. Rev. 37 (2008) 1967-1997.

[12] J. Muñiz, C. Wang, P. Pyykkö, Aurophilicity: The Effect of the Neutral Ligand *L* on $[\{ClAuL\}_2]$ Systems, Chem. Eur. J. 17 (2011) 368-377.

[13] H. Schmidbaur, S. Cronje, B. Djordjevic, O. Schuster, Understanding gold chemistry through relativity, Chem. Phys. 311 (2005) 151-161.

[14] H. Schmidbaur, A. Schier, Argentophilic interactions, Angew. Chem. Int. Ed. 54 (2015) 746-784.

[15] N. V. S. Harisomayajula, S. Makovetskyi, Y.-C. Tsai, Cuprophilic Interactions in and between Molecular Entities, Chem. Eur. J. 2019 (25) 8936-8954.

[16] H. Schmidbaur, A. Schier, Mercurophilic Interactions, Organometallics 34 (2015) 2049-2066.

[17] J. Echeverría, J. Cirera, S. Alvarez, Mercurophilic interactions: a theoretical study on the importance of ligands, Phys. Chem. Chem. Phys. 19 (2017) 11645.

[18] A. K. Pandey, M. Usman, S. P. Rath, Hg···Hg···Hg Interactions Stabilizes Unusual Trinuclear Double Sandwich Structure of Mercury(II) Porphyrins, Inorg. Chem. 59 (2020) 12988-12993.

[19] V. Vreshch, W. Shen, B. Nohra, S.-K. Yip, V. W.-W. Yam, C. Lescop, R. Réau, Aurophilicity versus Mercurophilicity: Impact of d^{10}-d^{10} Metallophilic Interactions on the Structure of Metal-Rich Supramolecular Assemblies, Chem. Eur. J. 18 (2012) 466-477.

[20] C. Cesari, B. Berti, F. Calcagno, C. Femoni, M. Garavelli, M. C. Iapalucci, I. Rivalta, S. Zacchini, Polymerization Isomerism in Co-M (M = Cu, Ag, Au) Carbonyl Clusters: Synthesis, Structures and Computational Investigation, Molecules 26 (2021) 1529.

[21] B. Berti, M. Bortoluzzi, C. Cesari, C. Femoni, M. C. Iapalucci, R. Mazzoni, S. Zacchini, A Comparative Experimental and Computational Study of Heterometallic Fe-M (M = Cu, Ag, Au) Carbonyl Clusters Containing N-Heterocyclic Carbene Ligands, Eur. J. Inorg. Chem. (2020) 2191-2202.

[22] B. Berti, M. Bortoluzzi, C. Cesari, C. Femoni, M. C. Iapalucci, R. Mazzoni, F. Vacca, S. Zacchini, Thermal Growth of Au-Fe Heterometallic Carbonyl Clusters Containing N-Heterocyclic Carbene and Phosphine Ligands, Inorg. Chem. 59 (2020) 2228-2240.

[23] B. Berti, M. Bortoluzzi, C. Cesari, C. Femoni, M. C. Iapalucci, L. Soleri, S. Zacchini, Synthesis, Structural Characterization, and DFT Investigations of $[M_xM'_{5-x}Fe_4(CO)_{16}]^{3-}$ (M, M' = Cu, Ag, Au; M ≠ M') 2-D Molecular Alloy Clusters, Inorg. Chem. 59 (2020) 15936-15952.

[24] B. Berti, M. Bortoluzzi, C. Cesari, C. Femoni, M. C. Iapalucci, R. Mazzoni, F. Vacca, S. Zacchini, Synthesis and Characterization of Heterobimetallic Carbonyl Clusters with Direct Au-Fe and Au···Au Interactions Supported by *N*-Heterocyclic Carbene and Phosphine Ligands, Eur. J. Inorg. Chem. (2019) 3084-3093.

[25] B. Berti, M. Bortoluzzi, C. Cesari, C. Femoni, M. C. Iapalucci, R. Mazzoni, F. Vacca, S. Zacchini, Polymerization Isomerism in $[\{MFe(CO)_4\}_n]^{n-}$ (M = Cu, Ag, Au; n = 3, 4) Molecular Clusters Supported by Metallophilic Interactions, Inorg. Chem. 58 (2019) 2911-2915.

[26] I. Ciabatti, C. Femoni, M. C. Iapalucci, S. Ruggieri, S. Zacchini, The role of gold in transition metal carbonyl clusters, Coord. Chem. Rev. 355 (2018) 27-38.

[27] M. Bortoluzzi, I. Ciabatti, C. Cesari, C. Femoni, M. C. Iapalucci, S. Zacchini, Synthesis of the Highly Reduced $[Fe_6C(CO)_{15}]^{4-}$ Carbonyl Carbide Cluster and Its Reactions with H^+ and $[Au(PPh_3)]^+$, Eur. J. Inorg. Chem. (2017) 3135-3143.

[28] M. Bortoluzzi, C. Cesari, I. Ciabatti, C. Femoni, M. Hayatifar, M. C. Iapalucci, R. Mazzoni, S. Zacchini, Bimetallic Fe-Au Carbonyl Clusters Derived from Collman's Reagent: Synthesis, Structure and DFT Analysis of $Fe(CO)(_4(AuNHC)_2$ and $[Au_3Fe_2(CO)_8(NHC)_2]^-$, J. Clust. Sci. 28 (2017) 703-723.

[29] C. Femoni, B. Berti, F. Calcagno, C. Lucarelli, M. Garavelli, R. Mazzoni, I. Rivalta, S. Zacchini, Bimetallic Co-M (M = Cu, Ag, Au) Carbonyl Complexes Supported by N-Heterocyclic Carbene Ligands: Synthesis, Structures, Computational Investigation, and Catalysis for Ammonia Borane Dehydrogenation, Organometallics 40 (2021) 2724-2735.

[30] S. Banerjee, M. K. Karunananda, S. Bagherzadeh, U. Jayarathne, S. R. Parmelee, G. W. Waldhart, N. P. Mankad, Synthesis and Characterization of Heterobimetallic Complexes with Direct Cu-M Bonds (M = Cr, Mn, Co, Mo, Ru, W) Supported by *N*-Heterocyclic Carbene Ligands: A Toolkit for Catalytic Reaction Discovery, Inorg. Chem. 53 (2014) 11307-11315.

[31] N. P. Mankad, Selectivity Effects in Bimetallic Catalysis, Chem. Eur. J. 22 (2016) 5822-5829.

[32] D. R. Pye, N. P. Mankad, Bimetallic catalysis for C-C and C-X coupling reactions, Chem. Sci. 8 (2017) 1705-1718.

[33] H.-C. Yu, N. P. Mankad, Catalytic Reactions by Heterobimetallic Carbonyl Complexes with Polar Metal-Metal Interactions, Synthesis 53 (2021) 1409-1422.

[34] N. P. Mankad, Diverse bimetallic mechanisms emerging from transition metal Lewis acid/base pairs: development of co-catalysis with metal carbenes and metal carbonyl anions, Chem. Commun. 54 (2018) 1291-1302.

[35] Y. Lakliang, N. P. Mankad, Heterometallic Cu_2Fe and Zn_2Fe_2 Complexes Derived from $[Fe(CO)_4]^{2-}$ and Cu/Fe Bifunctional N_2O Activation Reactivity, Organometallics 39 (2020) 2043-2046.

[36] J. Bauer, H. Braunschweig, R. D. Dewhurst, Metal-Only Lewis Pairs with Transition Metal Lewis Bases, Chem. Rev. 112 (2012) 4329-4346.

[37] J. Campos, Bimetallic Cooperation across the Periodic Table, Nat. Rev. Chem. 4 (2020) 696-702.

[38] I. G. Powers, C. Uyeda, Metal-Metal Bonds in Catalysis. ACS Catal. 7 (2017) 936-958.

[39] P. Buchwalter, J. Rosé, P. Braunstein, Multimetallic Catalysis Based on Heterometallic Complexes and Clusters, Chem. Rev. 115 (2015) 28-126.

[40] F. Schweyer, P. Braunstein, C. Estournès, J. Guille, H. Kessler, J.-L. Paillaud, J. Rosé, Metallic nanoparticles from heterometallic Co-Ru carbonyl clusters in mesoporous silica xerogels and MCM-41-type materials, Chem. Commun. (2000) 1271-1272.

[41] R. Paolillo, V. Gallo, P. Mastorilli, C. F. Nobile, J. Rosé, P. Braunstein, Tri- and Tetranuclear Homo- and Heterometallic Clusters as Precatalysts for the Pauson-Khand Reaction, Organometallics 27 (2008) 741-746.

[42] P. Buchwalter, J. Rosé, B. Lebeau, P. Rabu, P. Braunstein, J.-L. Paillaud, Stoichiometric molecular single source precursors to cobalt phosphides, Inorg. Chim. Acta 409 (2014) 330-341.

[43] R. D. Adams, B. Captain, Bimetallic cluster complexes: synthesis, structures and applications to catalysis, J. Organomet. Chem. 689 (2004) 4521-4529.

[44] R. D. Adams, F. A. Cotton (Eds.), Catalysis by Di- and Polynuclear Metal Cluster Complexes, Wiley-VCH, New York, 1998.

[45] G. Hogarth, S. E. Kabir, E. Nordlander, Cluster chemistry in the Noughties: new developments and their relationship to nanoparticles, Dalton Trans. 39 (2010) 6153-6174.

[46] M. Czaun, A. Goeppert, R. May, R. Haiges, G. K. S. Prakash, G. A. Olah, Hydrogen generation from formic acid decomposition by ruthenium carbonyl complexes. Tetraruthenium dedecacarbonyl tetrahydride as an active intermediate, ChemSusChem. 4 (2011) 1241-1248.

[47] A. F. Abdel-Magied, Y. Theibich, A. K. Singh, A. Rahaman, I. Doverbratt, A. K. Raha, M. Haukka, M. G. Richmond, E. Nordlander, Asymmetric hydrogenation of an α-unsaturated carboxylic acid catalyzed by intact chiral transition metal carbonyl clusters - diastereomeric control of enantioselectivity, Dalton Trans. 49 (2020) 4244-4256.

[48] S. Zacchini, Using Metal Carbonyl Clusters To Develop a Molecular Approach towards Metal Nanoparticles, Eur. J. Inorg. Chem. (2011) 4125-4145.

[49] S. Albonetti, R. Bonelli, R. Delaigle, C. Femoni, E. M. Gaigneaux, V. Morandi, L. Ortolani, C. Tiozzo, S. Zacchini, F. Trifirò, Catalytic combustion of toluene over cluster-derived gold/iron catalysts, Appl. Catal. A 372 (2010) 138-146.

[50] R. Bonelli, S. Zacchini, S. Albonetti, Gold/Iron Carbonyl Clusters for Tailored Au/FeO_x Supported Catalysts, Catalysts 2 (2012) 1-23.

[51] D. Bonincontro, A. Lolli, A. Storione, A. Gasparotto, B. Berti, S. Zacchini, N. Dimitratos, S. Albonetti, Pt and Pt/Sn carbonyl clusters as precursors for the synthesis of supported metal catalysts for the base-free oxidation of HMF, Appl. Catal. A 588 (2019) 117279.

[52] C. Cesari, J.-H. Shon, S. Zacchini, L. A. Berben, Metal carbonyl clusters of groups 8-10: synthesis and catalysis, Chem. Soc. Rev. 50 (2021) 9503-9539.

[53] H. Hock, H. Stuhlmann, Über die Einwirkung von Queksilbersalzen auf Eisenpentacarbonyl, Chem. Ber. 61 (1928) 2097-2101.

[54] H. W. Baird, L. F. Dahl, The crystal and molecular structure of $(BrHg)_2fe(CO)_4$, J. Organomet. Chem. 7 (1967) 503-214.

[55] Y.-K. Au, W.-T. Wong, Heterometallic Osmium-Mercury Chain Structures Linking Two $\{Os_3(CO)_{10}(\mu\text{-}X)\}$ Subunits (X = Cl, Br, I): Syntheses and Molecular Structures of $[\{Os_3(CO)_{10}(\mu\text{-}X)\}_2(\mu_4\text{-}Hg)]$ (X = Cl, I), $[\{Os_3(CO)_{10}(\mu\text{-}Cl)\}_2\{(\mu\text{-}Hg)Os(CO)_4\}_2]$, and *cis*-$[Os(CO)_4\{(\mu\text{-}Hg)Os_3(CO)_{10}(\mu\text{-}X)\}_2]$, Inorg. Chem. 36 (1997) 2092-2096.

[56] L. H. Gade, B. F. G. Johnson, J. Lewis, G. Conole, M. McPartlin, Redox-chemical core manipulation of $[Os_{18}Hg_3C_2(CO)_{42}]^{2-}$; synthesis and crystal structure of the cluster $[Os_{18}Hg_2C_2(CO)_{42}]^{4-}$, J. Chem. Soc., Dalton Trans. (1992) 3249-3254.

[57] E. Charalambous, L. H. Gade, B. F. G. Johnson, T. Kotch, A. J. Lees, J. Lewis, M. McPartlin, $[(Ph_3P)_2N]_2[Os_{18}Hg_2C_2(CO)_{42}]$ a Photochemically Generated High-Nuclearity Cluster Which Reversibly Incorporates Metallic Mercury into Its Metal Core, Angew. Chem. Int. Ed. 29 (1990) 1137-1139.

[58] C. A. Wright, U. Brand, J. R. Shapley, Synthesis and Characterization of the Dimercury(I)-Linked Compound $[PPN]_4[(Re_7C(CO)_{21}Hg)_2]$. Oxidative Cleavage of the Mercury-Mercury Bond Leading to $[PPN][Re_7C(CO)_{21}Hg(S{=}C(NMe_2)_2]$, Inorg. Chem. 40 (2001) 4896-4901.

[59] A. Albinati, A. Moor, P. S. Pregosin, L. M. Venanzi, Stabilization of Dimercury through Coordination to Platinum Cluster Units, J. Am. Chem. Soc. 104 (1982) 7672-7673.

[60] B. Berti, C. Femoni, M. C. Iapalucci, S. Ruggieri, S. Zacchini, Functionalization, Modification, and Transformation of Platinum Chini Clusters, Eur. J. Inorg. Chem. (2018) 3285-3296.

[61] M. Fajardo, H. D. Holden, B. F. G. Johnson, J. Lewis, P. R. Raithby, Synthesis and structural characterisation of the heteronuclear raft complex $[Os_3(CO)_{11}Hg]_3$, J. Chem. Soc., Chem. Commun. (1984) 24-25.

[62] L. H. Gade, B. F. G. Johnson, J. Lewis, M. McPartlin, T. Kotch, A. J. Lees, Photochemical core manipulation in high-nuclearity osmium-mercury clusters, J. Am. Chem. Soc. 113 (1991) 8698-8704.

[63] N. Masciocchi, P. Cairati, F. Ragaini, A. Sironi, *Ab Initio* XRPD Structure Determination of Metal Carbonyl Clusters: The Case of $[HgRu(CO)_4]_4$, Organometallics 12 (1993) 4499-4502.

[64] W. Gäde, E. Weiss, $[\eta^5\text{-}CH_3C_5H_4)Mn(CO)_2Hg]_4$, a Compound with an Mn_4Hg_4 Eight-Membered Ring and Additional Hg-Hg Bonds, Angew. Chem. Int. Ed. 20 (1981) 803-804.

[65] F. Glockling, V. B. Mahale, J. J. Sweeney, Organomercury complexes of iron, cobalt, and tungsten, J. Chem. Soc., Dalton Trans. (1979) 767-770.

[66] R. D. Ernst, T. J. Marks, J. A. Ibers, Metal-Metal Bond Cleavage Reactions. The Crystallization and Solid State Structural Characterization of Cadmium Tetracarbonyliron, $CdFe(CO)_4$, J. Am. Chem. Soc. 99 (1979) 2090-2098.

[67] H.-B. Song, Z.-Z. Zhang, T. C. W. Mak, 2,6-Bis(diphenylphosphino)pyridine-Bridged Hetero-Polynuclear Complexes Consolidated by Fe→M (M = Ag, Hg) Dative Bonding, Inorg. Chem. 40 (2001) 5928-5933.

[68] G. Chiaradonna, G. Ingrosso, F. Marchetti, $[\{Ir(\eta^5\text{-}C_5Me_5)(CO)\}_6Hg_8][CF_3CO_2]_6$, a Mixed-Metal Cluster with an Ir_6Hg_6 Twelve-Membered Ring and Additional Hg Centers and Metal-Metal Bonds, Angew. Chem. Int. Ed. 99 (2000) 3872-3873.

[69] A. Moreno, M. Haukka, M. Kallinen, T. A. Pakkanen, Reactions of $[Ru(CO)_3Cl_2]_2$ with aromatic nitrogen donor ligands in alcoholic media, Appl. Organomet. Chem. 20 (2006), 51-69.

[70] S. Ermer, K. King, K. I. Hardcastle, E. Rosenberg, A. M. M. Lanfredi, A. Tiripicchio, M. Tiripicchio-Camellini, Synthesis and Crystal Structure of Mercury-Bridged Transition-Metal Clusters: $Hg[Ru_3(CO)_9(C_2\text{-}t\text{-}Bu)]_2$ and $[(C_2\text{-}t\text{-}Bu)Ru_3(CO)_9HgMo(\eta\text{-}C_5H_5)(CO)_3]$, Inorg. Chem. 22 (1983) 1339-1344.

[71] P. L. Andreu, J. A. Cabeza, A. Liamazares, V. Riera, C. Bois, Y. Jeannin, Mercury-ruthenium mixed-metal carbonyl clusters containing 2-amido-6-methylpyridine (ampy) as a μ_3,η^2-ligand. Crystal structures of $[Ru_6(\mu_4\text{-}Hg)(\mu_3\text{-ampy})_2(CO)_{18}]\cdot 2C_4H_8O$ and $[Ru_3(\mu\text{-}HgBr)(\mu_3\text{-ampy})(CO)_9]$, J. Organomet. Chem. 420 (1991) 431-442.

[72] A. Bianchini, L. J. Farrugia, Synthesis and Dynamic Behavior of Mercury-Linked Clusters Containing Methoxymethylidyne Ligands: X-ray Structures of $Hg[Fe_2M(\mu_3\text{-}COCH_3)(CO)_7(\eta\text{-}C_5H_5)_2$ (M = Co, Rh), $Hg[Ru_3(\mu\text{-}COCH_3)(CO)_{10}]_2$, and $Hg[Fe(CO)_4(\mu\text{-}Hg)Fe_3(\mu\text{-}COCH_3)(CO)_{10}]_2$, Organometallics 11 (1992) 540-548.

[73] J. Liu, E. P. Boyd, S. G. Shore, The $[Ru_3(CO)_{11}]^{2-}$ dianion, Acta Cryst. C55 (1999) 29-30.

[74] F. A. Cotton, L. M. Daniels, C. A. Murillo, H. C. Zhou, The Effect of Divergent-Bite Ligands on Metal-Metal Bond Distances in Some Paddlewheel Complexes, Inorg. Chim. Acta 300-302 (2000) 319-327.

[75] L. Pauling, Atomic Radii and Interatomic Distances in Metals, J. Am. Chem. Soc. 69 (1947) 542-553.

[76] S. R. Parmelee, N. P. Mankad, A data-intensive re-evaluation of semibridging carbonyl ligands, Dalton Trans. 44 (2015) 17007-17014.

[77] M. D. P. Mingos, R. L. Jonston, Theoretical models of cluster bonding, Struct. Bonding (Berlin) 68 (1987) 29-87.

[78] R. Bianchi, G. Gervasio, D. Marabello, Experimental Electron Density Analysis of $Mn_2(CO)_{10}$: Metal-Metal and Metal-Ligand Bond Characterization, Inorg. Chem. 39 (2000) 2360-2366.

[79] C. Lepetit, P. Fau, K. Fajerwerg, M. L. Kahn, B. Silvi, Topological analysis of the metal-metal bond: A tutorial review, Coord. Chem. Rev. 345 (2017) 150-162.

[80] F. Mendizabal, S. Miranda-Rojas, L. Barrientos-Poblete, A comparative study between post-Hartree-Fock methods and density functional theory in closed-shell aurophilic attraction, Comput. Theor. Chem. 1057 (2015) 74-79.

[81] C. Cesari, M. Bortoluzzi, C. Femoni, M. C. Iapalucci, S. Zacchini, Synthesis, molecular structure and fluxional behavior of the elusive $[HRu_4(CO)_{12}]^{3-}$ carbonyl anion, Dalton Trans. 51 (2022) 2250-2261.

[82] C. Cesari, M. Bortoluzzi, C. Femoni, M. C. Iapalucci, S. Zacchini, One-pot atmospheric pressure synthesis of $[H_3Ru_4(CO)_{12}]^-$, Dalton Trans. 50 (2021) 9610-9622.

[83] N. E. Kolobova, Z. P. Valueva, E. I. Kazimirchuk, V. G. Andrianov, Yu. T. Struchkov, Synthesis and some properties of tetra[η^5-cyclopentadienyldi-carbonylrheniummercury], Russ. Chem. Bull. 22 (1984) 847-850.

[84] P. Michelin Lausarot, G. A. Vaglio, M. Valle, A. Tiripicchio, M. Tiripicchio-Camellini, P. Gariboldi, Activation of the carbon-nitrogen triple bond of benzonitrile in the presence of triosmium clusters and acetic acid. Crystal structure of (μ-H)$Os_3(CO)_{10}$(μ-O_2CCH_3), a product of the reaction, J. Organomet. Chem. 291 (1985) 221-229.

[85] G. R. Frauenhoff, S. R. Wilson, J. R. Shapley, Isolation, Characterization, and Substitution Reactions of the Trinuclear Triflate Complex $H_2Os_3(CO)_9(O_3SCF_3)$. X-ray Crystal Structure of the Mixed Oxy Ligand Cluster (μ-H)$_2Os_3(CO)_9$(μ,η^2-O_2CCH_3)(η^1-O_3SCF_3), Inorg. Chem. 30 (1991) 78-85.

[86] P. Teulon, J. Roziere, Synthesis and structural characterization of the molecular complex $[Ru(CO)_3Cl_2]_2 \cdot SbCl_3$, J. Organomet. Chem. 214 (1981) 391-397.

[87] E. Keller, *SCHAKAL99*; University of Freiburg: Freiburg, Germany, 1999.

[88] G. M. Sheldrick, *SADABS-2008/1-Bruker AXS Area Detector Scaling and Absorption Correction*; Bruker AXS: Madison, WI, 2008.

[89] G. M. Sheldrick, Crystal Structure Refinement with SCHELXL, Acta Crystallogr., Sect. C: Struct. Chem. 71 (2015) 3-8.

[90] A. L. Spek, Single-crystal structure validation with the program PLATON, J. Appl. Cryst. 36 (2003) 7-11.

[91] S. Grimme, J. G. Brandenburg, C. Bannwarth, A. Hansen, A. Consistent structures and interactions by density functional theory with small atomic orbital basis sets, J. Chem. Phys. 143 (2015) 054107.

[92] F. Weigend, R. Ahlrichs, Balanced basis sets of split valence, triple zeta valence and quadruple zeta valence quality for H to Rn: Design and assessment of accuracy, Phys. Chem. Chem. Phys. 7 (2005) 3297-3305.

[93] D. Andrae, U. Haeussermann, M. Dolg, H. Stoll, H. Preuss, Energy-adjusted ab initio pseudopotentials for the second and third row transition elements, Theor. Chim. Acta 77 (1990) 123-141.

[94] F. Weigend, Accurate Coulomb-fitting basis sets for H to Rn, Phys. Chem. Chem. Phys. 8 (2006) 1057-1065.

[95] H. Kruse, S. Grimme, A geometrical correction for the inter- and intra-molecular basis set superposition error in Hartree-Fock and density functional theory calculations for large systems, J. Chem. Phys. 136 (2012) 154101.

[96] S. Grimme, S. Ehrlich, L. Goerigk, Effect of the damping function in dispersion corrected density functional theory, J. Comput. Chem. 32 (2011) 1456-1465.

[97] S. Grimme, J. Antony, S. Ehrlich, H. Krieg, A consistent and accurate ab initio parametrization of density functional dispersion correction (DFT-D) for the 94 elements H-Pu, J. Chem. Phys. 132 (2010) 154104.

[98] M. Cossi, N. Rega, G. Scalmani, V. Barone, Energies, structures, and electronic properties of molecules in solution with the C-PCM solvation model, J. Comput. Chem. 24 (2003) 669–681

[99] V. Barone, M. Cossi, Quantum Calculation of Molecular Energies and Energy Gradients in Solution by a Conductor Solvent Model, J. Phys. Chem. A 102 (1998) 1995–2001

[100] F. Neese, Software update: The ORCA program system - Version 5.0, WIREs Comput. Mol. Sci. (2022) e1616.

[101] T. Lu, F. Chen, Multiwfn: A multifunctional wavefunction analyzer, J. Comput. Chem. 33 (2012) 580-592.